2009

Voltage security assessment with high penetration levels of utility-scale doubly fed induction generator wind plants

Ryan Konopinski
Iowa State University

Voltage security assessment with high penetration levels of utility-scale doubly fed induction generator wind plants

by

Ryan Konopinski

A thesis submitted to the graduate faculty

in partial fulfillment of the requirements for the degree of

MASTER OF SCIENCE

Major: Electrical Engineering

Program of Study Committee:
Venkataramana Ajjarapu, Major Professor
Chen-Ching Liu
Douglas Gemmill

Iowa State University

Ames, Iowa

2009

TABLE OF CONTENTS

LIST OF FIGURES

LIST OF TABLES

CHAPTER 1. INTRODUCTION

This work details the impact and development of utilizing a capability curve for a doubly fed induction generator (DFIG) wind plant. The steady state and dynamic power system response to the reactive capability of the machines are tested with high wind penetration levels. This work was motivated by the interconnection requirements set forth by FERC in order 661-A which mandate the operation of wind parks within a power factor range of 0.95 leading and lagging. This restricted operation drastically under-utilizes the reactive output of the machine and hence creates a potential negative impact to the power system.

The results presented in this work outline a methodology for determining the penetration level of a system based on voltage and power transfer criteria defined for the system. DFIG wind model control enhancements were also developed which improve post fault voltage profiles and damp system swings, preventing overshoot immediately after a disturbance. In the presented case study the extended reactive limits of the plant were found to prevent system collapse.

1.1 Trends, Regulation, and Concerns with Wind Generators

In today's world, with rising global fuel prices and concerns relating to climate change, there is an increasing focus on renewable sources to satisfy energy requirements. Among the renewable resources, wind generation is gaining prominence due to available technologies that allow for large-scale power generation [1], [2]. The year 2007 was a record

year for wind generation in the United States with a total increase of 45% in wind installations that accounted for 30% of all newly added generation [3], [4].

Federal policy in the form of production tax credits and state regulations in the form of renewable portfolio standards (RPS) [5] have contributed to encouraging the development of wind generation in the United States [6]. Over 25 states have accepted RPS by requiring a substantial contribution from renewables to their power generation portfolio [7]. Considering these incentives and mandates, wind generation technology appears to be the most popular renewable option for developers. Although, the same types of regulatory policy that is helping stimulate construction, may be counter productive to power system operation.

In 2005, FERC orders 661 and 661-A [23] [24] were released which mandate the interconnection requirements for large wind parks over 20MW. According to this order, a key requirement for plant operation is that the power factor at the point of interconnection (POI) must remain between 0.95 leading and 0.95 lagging. Reference [24] states that the reason for this ruling is that reactive power capability for a wind plant is a significant additional cost compared to conventional units that possess inherent reactive capability. As more wind installations appear in years to come, policy rulings may need modification to allow for healthy performance of the power system.

The majority of the newly installed wind generation consists of doubly fed induction generators, but it has not always this way [8]. Figure 1 shows the percentage of the different types of wind turbines installed each year from 1995 through 2005. There are four types of wind units: type A – Fixed Speed (FSG), type B – FSG with Variable Rotor Resistance (WRIG), type C – Doubly Fed Induction Generators (DFIG), and type D – Full Scale Frequency Converter (WRSG).

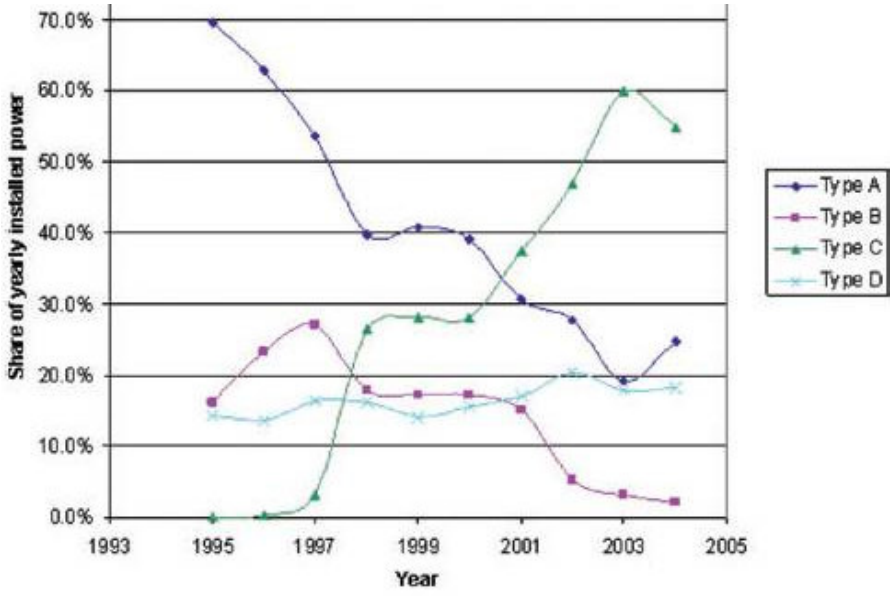

Figure 1. Yearly installed types of turbines by percentage from 1995-2005 [8]

It should be noted that traditional wind generating units (type A&B) do not possess reactive capability. They were, contrast to DFIG units, reactive power consumers whose inherent downfall lead to the inability to regulate terminal voltage [51]. To mitigate this reactive demand, many FSG and WRIG wind parks were equipped with external sources of reactive power. Static source installations such as shunt capacitors are relatively inexpensive as compared to dynamic resources such as SVCs [18]. On the other hand, newer wind parks consisting of DFIG units have reactive power capability [19]. The presence of power electronic controls in DFIGs makes them a fast acting dynamic reactive resource as compared to synchronous generators [20]. This allows for voltage regulation and reactive power control by a wind park [21], [22]. As more and more DFIGs come online, the threat of increasing levels of wind penetration have generated a widespread concern over potential impacts to power system performance.

There are primarily two reasons for such a concern, the variability of the resource and the nature of the generator, both of which imply the restructuring of system operation and the inclusion of non-traditional system equipment [9]. Therefore, the effect of high wind penetration levels on system performance becomes a critical factor in power system operation and planning of future units. To accommodate this new style of generation, precise modeling of DFIG units is important for both static and dynamic analysis of power system performance [1]. When considering performance criterion, system frequency and voltage levels must be maintained within strict tolerance for proper operation [53]. Compared to other turbine configurations DFIG wind units possess the superiority to operate during low voltage conditions as well as regulate system voltage levels [52]. Therefore, it was decided to study the system impact of DFIG wind turbines with a focus on the voltage regulating features within the machine.

The following work demonstrates reliability improvements in both static and dynamic power system operation through application of an extended capability curve. It is shown that, contrary to FERC order 661-A, DFIG wind parks may and should operate at much lower power factors without incurring additional costs to the plant owner. This extended reactive capability allows for not only improved voltage recovery following a grid disturbance, but may aid in the prevention of a system collapse. The results provide valuable information that help to accurately assess the stability of a system and to prevent voltage violations with studies involving high penetration levels [10].

It will be shown that imposing this power factor restriction limits the performance of DFIG wind parks, which directly influence the system performance. Thus utilizing the DFIG capability curve can lead to improved static and dynamic system response as well as reduce

the amount of committed conventional reactive reserve. The FERC order 661-A gives general guidelines for interconnecting wind parks, but for specific parks employing DFIG units the restriction on power factor should be lifted because additional performance may be obtained at no extra cost to the wind farm owner.

1.2 Fundamentals of Doubly Fed Induction Generators

Doubly fed induction generators are a type of variable speed wind turbine that include operational advantages of both synchronous and induction machines. As with any induction machine variable speed operation can easily be achieved. In DFIG turbines this feature allows the capture of maximum wind potential over a wide range of wind speeds using a control strategy termed maximum power tracking (MPT). This tracking characteristic is accomplished by regulating the power extracted by the rotor blades at a given operating speed from the wind [54]. The MPT superiority is observed economically when compared to a fixed speed turbine with upwards of a 10% increase in energy efficiency [1].

Figure 2 lays out a high level diagram that contains the systems and subsystems involved with a DFIG machine. As with other electrical machines, DFIGs have both electrical and mechanical components. The main mechanical system contains rotor blades that are fixed to a prime mover that are controlled with a pitching mechanism to adjust the associated aerodynamic characteristics. The prime mover then connects to a step up gearbox that drives the generator. The electrical system is comprised of a wound rotor induction generator and power electronic converter (PEC) control that functions as the generator exciter [55].

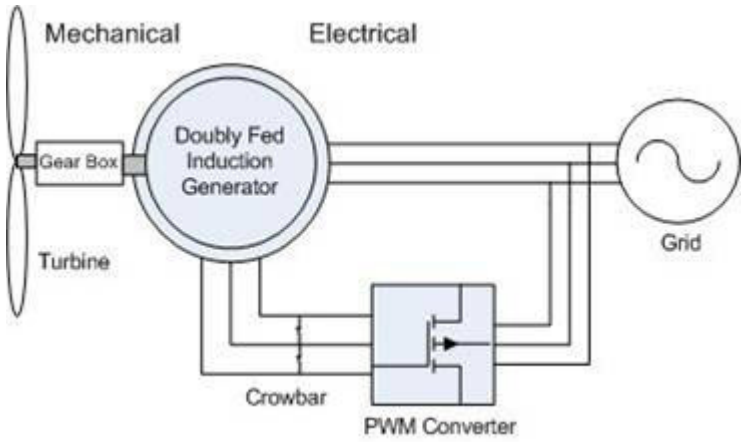

Figure 2. High-level system overview of a DFIG wind turbine

Since the PEC acts as the machines excitation system, complete control of reactive power is handled here. This is accomplished through a back-to-back converter that couples the rotor windings of the machine to the grid side of the machine. Figure 3 displays the converter architecture that consists of IGBT controlled switches that have a common DC bus linking the AC circuits [56].

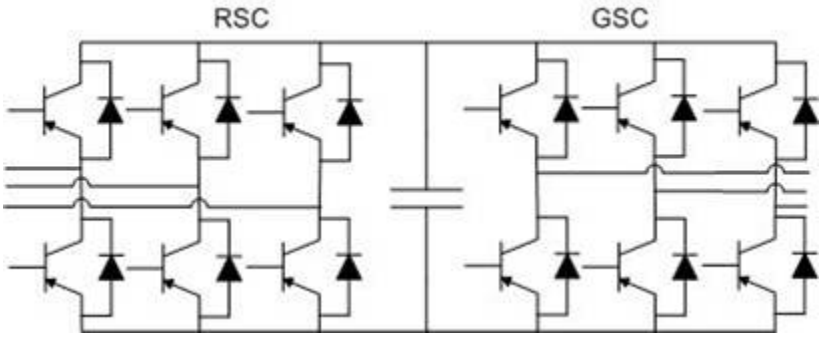

Figure 3. Power electronic converter architecture

As such the PEC is comprised of two independently controlled three-phase inverters that can function in four-quadrant operation. The names of these converters will be referred to as the RSC and GSC, which are the respective rotor and grid side converters. The back-to-back

RSC and GSC configuration allows for bi-directional power flow between the rotor side windings and the stator side output terminals of the machine. This system of power transfer resembles an HVDC set up wherein two asynchronous systems are interconnected. This versatility lends itself to the nature of the machine as the mechanical speed is constantly changing with fluctuations in the wind. Therefore, in order to maintain an internal rotating magnetic field with respect to the grid frequency (as in synchronous machines) the RSC is constantly adjusting its current injections to the rotor. Thus, excitation of the generator is supplied by the RSC shown in Figure 4. The frequency of the current injections is defined by equations 1.

$$\omega_s = \omega_r + \omega_m \tag{1}$$

In this manner the RSC maintains a rotating magnetic field at synchronous speed ω_s by injecting currents at a frequency ω_r given the mechanical rotation of the machine ω_m.

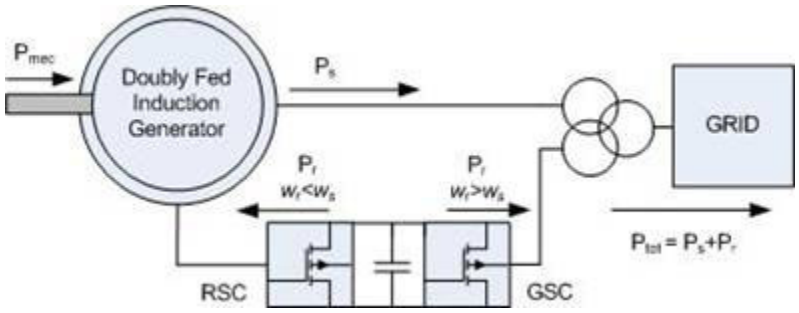

Figure 4. DFIG high level power balance schematic

Figure 4 also shows the flow of power within the machine, where the total mechanical, stator and rotor electrical powers are respectively defined by P_m, P_s, P_r. Since the generator is an induction machine the slip (s) is given by:

$$s = \frac{\omega_s - \frac{p}{2}\omega_m}{\omega_s} \tag{2}$$

where p is the number or poles. Relations of the above powers can be approximately expressed using the slip of the machine to derive the total electrical real (P_{tot}) power output.

$$P_{tot} = P_s + P_r \approx P_m \approx P_s(1-s) \tag{3}$$

The next chapter will present details regarding the derivations of the total electrical active and reactive capability from the machine and power electronic converters.

CHAPTER 2. STATIC MODELING OF DFIG WIND PLANTS

References [34], [35] make claims of 20% penetration levels from wind resources in the U.S. At these levels, misrepresenting the actual power capability of DFIG plants at high penetration levels may cause large discrepancies between the actual power flows and misrepresent limits on the power system. Although DFIG parks may be modeled in various ways, considering the true reactive ability of the plant is paramount for studying future system operation.

Power flow simulations are used to derive bus voltages and network line flows for given load conditions. Typically generating units are modeled with a finite operating region for real and reactive power outputs. In recent years appropriate representation of wind plants have been of increasing interest.

2.1 Introduction

Proper machine modeling is necessary to understand the actual reactive power capability of a DFIG wind park. These machines can be represented using the simplified traditional induction machine T-model (figure 5) with an additional voltage source connected to the rotor. This voltage source represents the rotor side converter (RSC) that excites the machine.

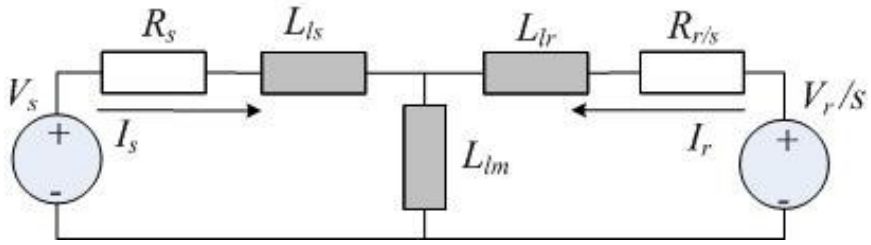

Figure 5. DFIG static machine model

In the above figure the stator and rotor voltage (V_s, V_r) and flux (ψ_s,ψ_r) equations can be derived from the machine currents (I_s, I_r) [25]. In equations 4-7, (R_s,L_{ls}) and (R_r, L_{lr}) are the respective stator and rotor resistance and leakage inductance with L_{lm} defining the magnetizing inductance.

$$V_s = (R_s + j\omega_s L_s)I_s + j\omega_s L_m (I_s + I_r) \tag{4}$$

$$\frac{V_r}{s} = \left(\frac{R_r}{s} + j\omega_s L_r\right)I_r + j\omega_s L_m (I_s + I_r) \tag{5}$$

$$\psi_s = L_s I_s - L_{lm} I_r \tag{6}$$

$$\psi_r = L_r I_r - L_{lm} I_s \tag{7}$$

The grid frequency is given by w_s, the machine slip is s, and L_s=L_{ls}+L_{lm} and L_r=L_{lr}+L_{lm}.

The RSC size is computed from the ratings of the rotor side voltage source by combining the above basic KVL loop equations with the stator and rotor flux equations. Eliminating the stator flux from these equations, expressions for the rotor current, voltage, and converter MVA rating can be computed [25].

$$I_r = (\psi_r - L_m I_s)/L_r \tag{8}$$

$$V_r = \psi_r[(R_r/L_r) + j\omega_s s] - [I_s(L_m/L_r)R_r] \tag{9}$$

$$S_r = 3\left|(V_r I_r^*)\right| \tag{10}$$

The converter that excites the DFIG machine is constructed with a back-to-back power electronic converter (PEC) that is fed from a DC voltage source [26]. Given the

highest AC voltage connected to the bi-directional converter the DC link voltage can be obtained using the following relation where P_m is the modulation index.

$$V_{dc-link} = \frac{2\sqrt{2}}{\sqrt{3}P_m} V_{ac} \tag{11}$$

2.1.1 DFIG Plant Capability Curve

It is well known that electro-mechanical machines have inherent limitations that allow for a fixed amount of power production. The operating characteristics of any generator are important for representing a machine's true power capability. The limitations that define a DFIGs electrical power capability are influenced by two factors – the generator and power electronics. Referring to the maximum power tracking characteristic (Appendix A) it should be noted that only a finite amount of power is able from a given wind speed. Therefore the real power limits are set by the availability of the wind. The maximum reactive capability of the machine is determined by the generator design where the applied currents and voltages set limitations on the stator and rotor. Therefore, the maximum power capability is completely limited by the design of the machine although the back-to-back power converter, which will be addressed in section 2.1.4, defines the actual capability.

A capability curve for a DFIG wind park was formulated using the method followed in [31] with a maximum power tracking characteristic given in Appendix A. This technique is given for only a single machine, but it is assumed that the power capability of one machine can be scaled up to accurately aggregate the behavior of a DFIG wind park.

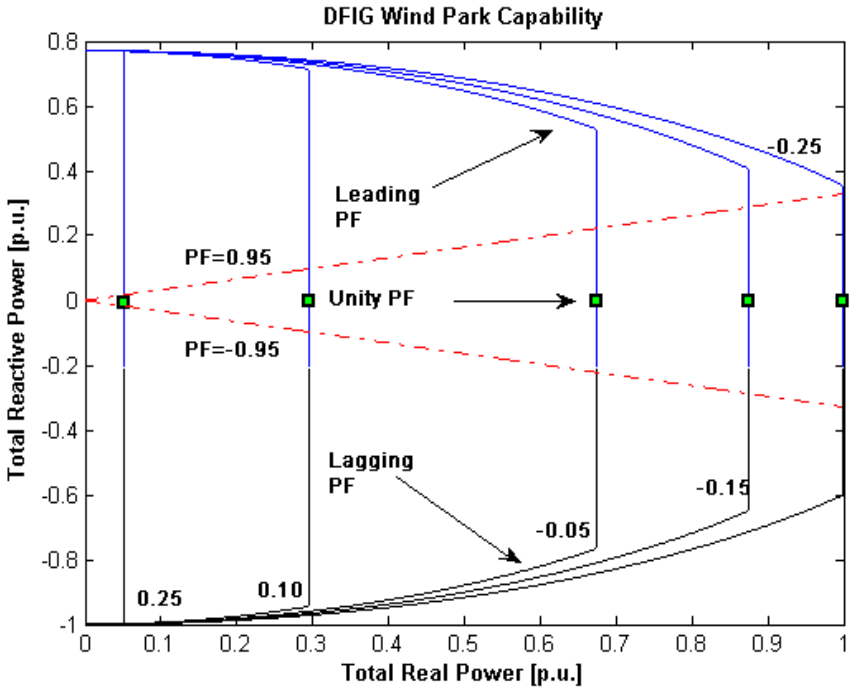

Figure 6. DFIG wind park static power capability curve in per units

This is made under the assumption that the DFIG wind park network is not considered such as each machine feeder line and transformer. Additional impedance may be added to the model, which accounts for these simplifications [32].

The plot in figure 6 displays the operation of a DFIG within the specified 0.95 leading and 0.95 lagging power factors. Superimposed is the capability curve for the DFIG at different wind speeds corresponding to variable levels of power output. Given in the plot are the capability curves for slips 0.25, 0.1, -0.05, -0.15 and -0.25. This spans the entire spectrum of wind speeds from cut-in speed that corresponds to 0.25 slip to just before cut-out speed that corresponds to -0.25 slip. Thus by utilizing the capability curve in network analysis additional reactive power and hence improved power system performance may be attained over a regulated power factor. It is evident from the figure that at 100% plant output the use

of the capability curve does not give much additional reactive support compared to the 0.95 leading operation. In contrast additional reactive consumption may be realized in lagging operation. Wind parks will never continuously operate at 100% output and therefore in the periods of operation below 100% there is significant additional reactive power available that could aid in improved system performance.

2.1.2 DFIG Wind Park Load Flow Models

For any power system analysis it is important to appropriately model the characteristics of a system device. In the case of DFIG machines and machines that make up the response of a DFIG wind park, models for static analysis are still being developed. The following section will briefly discuss several model representations of DFIG wind plants.

2.1.2.1 Negative Load Representation

One of the most simplified DFIG wind park representations can be defined by a negative load [36]. During the load flow this representation will inject real power (P) and either leading or lagging reactive power (+/-Q) into the grid. The farm is modeled as a PQ bus. This model assumes that the wind farm operates at a fixed power factor and cannot regulate its reactive output.

2.1.2.2 Synchronous Machine Representation

A wind park may be modeled as a synchronous generator with either fixed real and reactive power limits or by employing a capability curve. Both models are representative of a PV bus that contains terminal voltage control. The capability curve is the more accurate representation. The only disadvantage of this strategy is that the steady state set points cannot

directly be used in dynamic simulations. Therefore, the initial set points must be recomputed for the dynamic DFIG models.

2.1.2.3 DFIG Representation

Several software manufacturers now appropriately account for DFIG wind park models in load flow studies. Notable are PSS/E [37], [38], PowerFactory [30], and Eurostag [39] simulation software for including models that can automatically be initialized for dynamic analysis. For the strict purpose of steady state analysis, synchronous machine representation can accurately portray the behavior of a wind plant. As such, employing a DFIG capability curve using a synchronous machine model proves advantageous when studying high levels of wind penetration.

2.1.3 Wind Park Aggregation

Although models of DFIG turbines have been well studied [27] there is no industry standard and as such each software package may contain its own DFIG model. Moreover since larger scale wind parks will contain upwards of several hundred units, modeling of individual units for power system dynamic studies would result in large simulation times and require greater computation capability. Therefore model simplification and park aggregation is justified in certain power system analysis.

The inclusion of a wind farm into a power system for simulation purposes is often best represented by a condensed model. Aggregation techniques of variable speed wind turbines have been thoroughly discussed and their significance described in [28]. Studies

comparing the results between detailed and aggregated models conclude that an aggregated electrical system and non-aggregated mechanical system is an efficient and accurate model for mid and long term simulations [29]. For short-term simulations both electrical and mechanical systems may be aggregated.

For the purpose of dynamic simulation, an aggregated park of approximately 100 DFIG units was modeled in PowerFactory simulation software by DIgSILENT [30]. The park was constructed with a fully aggregated technique that condenses the behavior of each individual turbine's electrical and mechanical models into a single machine model representing both electrical and mechanical characteristics.

2.1.4 Reactive Capability Validation

The DFIG parks used in this study are 1.5 MW units that contain a power electronic converter rated to 30% of the machine rating (Appendix B). This assumption is justified by calculating and comparing the required PEC rating necessary to operate between a +/- 0.95 power factor as well as over the entire range of the capability curve in figure 6. The procedure outlined in [25] was followed to compute I_r, V_r, V_{dc}, and S_{conv} corresponding to several operating points given respective active and reactive powers. Rows 1-5 of table 1 detail the converter calculations for several operational points taken from the DFIG capability curve. Row 6 shows the ratings necessary to operate at 0.95 leading power factor at rated output. Observe in figure 6 that at each real power (P) operating point the reactive limitation (Q) of the restricted power factor regulation is less than the capability curve (except near 100% real output). It is apparent in table 1 that as the DFIG active output (P_{tot})

increases likewise does the current magnitude (I_r). Near 50% output the machine reaches its synchronous speed and the voltage applied to the rotor is minimal and therefore the required converter rating is at its lowest. Near 100% output the required rotor current, voltage, and converter ratings are at their highest value. This implies that the leading reactive output (Q_{tot}) determines the converter ratings and size at 100% output. Hence, only the maximum operating point for the power factor regulation was displayed.

Table 1. Converter Sizing for Theoretical Reactive Operation

	P_{tot} [p.u.]	Q_{tot} [p.u.]	slip [%]	V_{rotor} [V]	I_{rotor} [A]	$V_{dc\text{-}link}$ [V]	$S_{converter}$ [kVA]
1	0.05	0.80	25.26	244	352	440	258.5
2	0.25	0.72	11.50	108	449	195	146.2
3	0.50	0.63	1.33	8	425	14	10.2
4	0.75	0.49	-9.28	97	428	175	125.4
5	1.00	0.37	-25.14	254	468	460	357.9
6	*1.00*	*0.33*	*-25.14*	*254*	*458*	*460*	*348.6*

The required DC link capacitor voltage based on the stator side voltage is calculated using equation 11 with a maximum modulation index of 0.9. The stator side rated voltage is 575 V and therefore the corresponding DC link voltage is 938 V. From the above table the required $V_{dc\text{-}link}$ from the rotor side voltage is lower compared to that required by the stator side voltage. This implies that no change in the actual DC link capacitor voltage rating is necessary to implement the capability curve. The implemented PEC rating was derived using a margin of safety based on the highest kVA rating from table 1. The DC capacitor voltage was designed from the stator side voltage and rated to 1150 V with the PEC rated at 450 kVA.

It is very important to note that operation of a DFIG with a power factor regulation must produce a Q_{tot} of 0.33 and for the capability curve it must produce 0.37 at rated active power. Comparing I_r and $S_{converter}$ for rows 5 and 6 in table 1 show that only a 2% increase in the ratings is necessary to implement this capability curve over a regulated power factor scheme. Therefore converters installed in operational and newly commissioned DFIG wind farms abiding by the FERC 661-A orders have additional reactive capability that may be utilized. This demonstrates that operating the DFIG within a power factor regulation greatly under-utilizes the machines overall reactive ability.

CHAPTER 3. DFIG PLANT DYNAMIC MODELING AND CONTROL

To ascertain the dynamic performance of a power system with large amounts of DFIG wind penetration, appropriate modeling of DFIG wind parks is necessary. Each machine in a wind park has several sub system models in order to accurately reproduce the response of each machine. Since wind parks are made up of any where from several to hundreds of turbines, steps must be taken to lump the individual responses into one large or aggregated model that represents the behavior of the wind park. The sub systems that will be discussed in this chapter are the aerodynamic, mechanical, electrical, and control subsystems that comprise the DFIG wind turbine system. The block diagram of the DFIG machine that relates the all the systems and sub systems is displayed in Figure 7.

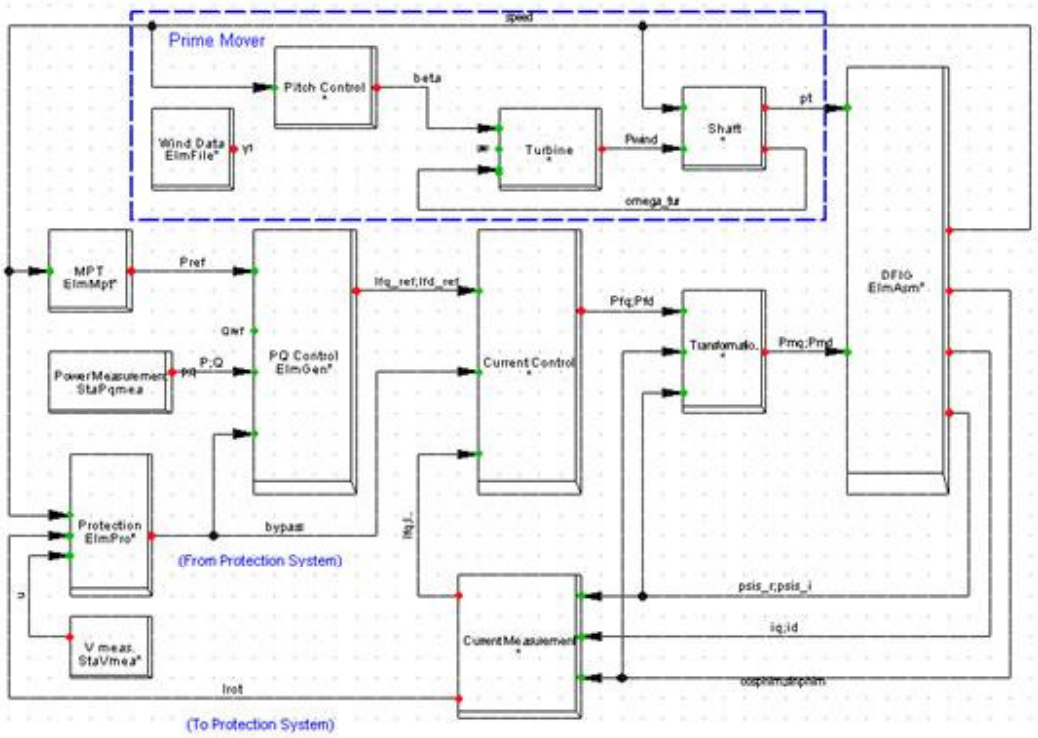

Figure 7. DFIG Main Block Diagram [30]

3.1 Dynamic Modeling Principles

All wind turbines perform the function of converting mechanical to electrical energy for transportation via the electric transmission network. The energy conversion process begins with the energy input source: the wind, which obeys certain aerodynamic characteristics. The following section introduces the principles of how a turbine extracts power from the wind.

3.1.1 Aerodynamic Characteristics

As wind flows past the blades of a machine, whether rotating or stationary, mechanical lift is produced and an aerodynamic torque (T_{ae}) is applied to the blades. Depending on the rotation of the blades, this torque produces a mechanical power (P_m). The mechanical power that the turbine extracts from the wind and applied to the electrical subsystem for conversion is given by the following relationship

$$P_m = \tfrac{1}{2} cp(\lambda, \beta) \pi \rho_{air} R^2 V_w^3 \tag{12}$$

This power (Pm) is function of the speed of the wind (V_w), the blade radius (R), the density of the air (ρ_{air}), and the performance coefficient of the rotor blades (cp).

Due to the physical nature of the energy capturing process, not all the power available from the wind may be extracted by the turbine blades as described by Betz' law [57]. This fact is quantitatively illustrated as the performance coefficient of the rotor (cp). It is a manufacturer specified parameter that is determined from a method outlined in [57]. The performance coefficient is a highly non-linear variable defined by a function based on the parameters (λ, β) as shown in 12.

The tip-speed ratio (λ) is given in equation 13 as the speed at the tip of the rotor blade divided by the upstream wind velocity (V_w) where $\omega_{r,tur}$ is the angular speed of the turbines rotor.

$$\lambda = \frac{\omega_{r,tur} R}{V_w} \tag{13}$$

The parameter β is the pitch angle of the rotor blades with units in degrees. The pitch angle of the turbine blades can be controlled to influence the value of *cp*, which in turn limits the amount of mechanical power available for extraction from the wind.

Figure 8 presents a graphical representation of *cp* with respect to a continuously varying λ over different discrete values of β. From this plot it can easily be observed as the pitch angle (β) increases the performance coefficient is reduced and thus decreases the extracted power from the wind. S. Heier explains how to analytically calculate the performance coefficient of a wind turbine [57].

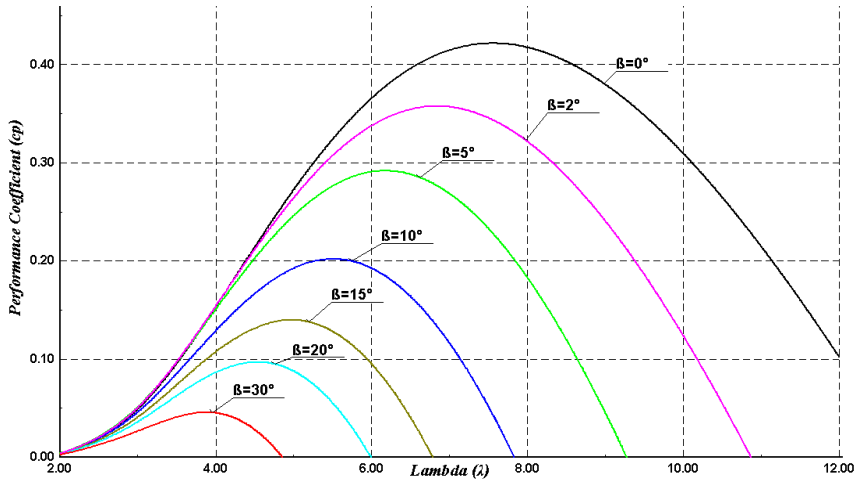

Figure 8. Rotor performance coefficient *cp* vs. tip-speed ratio λ for various pitch angles β

Using this method, equations 14 and 15 were derived and the above rotor performance coefficient curves were developed for the DFIG model used in this study. It should be noted that a turbines mechanical power depends on *cp* and therefore is deemed a design parameter.

$$C_p(\lambda,\beta) = 0.71\left(\frac{150}{\lambda_i} - 0.6\beta - 0.002\beta^{0.14} - 13.2\right)e^{\left(\frac{-18.4}{\lambda_i}\right)} \tag{14}$$

$$\lambda_i = \left[\left(\frac{1}{\lambda - 0.002\beta}\right) - \left(\frac{-.01}{\beta^3 + 1}\right)\right]^{-1} \tag{15}$$

Since the calculation of these curves can be computationally cumbersome with an explicit function, discrete points from (λ,β) indices may be defined by a two-dimensional lookup table (A).

$$cp(\lambda,\beta) = \mathrm{A}_{\lambda,\beta} \tag{16}$$

For values not located in discrete entries of the table an interpolation method, such as a cubic spline function, may be used to determine these points. Thus, the aerodynamic curves developed in MATLAB were then entered as discrete input points into the dynamic simulation software.

3.1.2 Mechanical Drive Train Characteristics

The mechanical system of the Doubly Fed machines used in this project only model the dynamic response of the drive train inertias. These simplifications are made due to the fact that the drive train has the most significant impact on power fluctuations [59]. Any other mechanical elements are thus not considered in this model. Additionally, the mechanical

model is more general in nature and may apply to any type of wind turbine. As such, the purpose of the drive train is to convert the aerodynamic torque (T_{ae}) from the wind into mechanical torque on the low speed shaft (T_{shaft}) that couples to the generator via a gearbox [58]. The gearbox is assumed to be lossless with a gear ratio of 1:n_{gear}.

PowerFactory simulation software considers a two mass lumped model with one large mass symbolizing the rotor inertia and a smaller mass representing the generator inertia [55]. These general details regarding the drive train lead to expressions for the system of equations that make up the mechanical model [60].

$$2H_m\dot{\omega}_m = T_m - k\theta_{mg} - D_m\omega_m \tag{17}$$

$$2H_g\dot{\omega}_g = k\theta_{mg} - T_e - D_g\omega_g \tag{18}$$

$$\dot{\theta}_{mg} = \omega_o(\omega_m - \omega_g) \tag{19}$$

T_m is the accelerating torque from the wind and T_e is the decelerating electric torque. K is the shaft stiffness and θ_{mg} is the angular torsion in the shaft. $D_m\omega_m$ and $D_g\omega_g$ are the damping torques of the turbine and generator where $\omega_o, \omega_m, \omega_g$ are the system, rotor, and generator speeds. This system of differential equations comprises the two-mass drive train model used in the simulations.

3.1.3 Generator Characteristics

The electrical system is made up of a system of differential equations modeling the dynamic response of the DFIG machine. The differential equations that make up this machine are very similar to that of a traditional induction machine, but do not contain short-

circuited rotor windings. Instead a voltage source generated by the RSC is connected to the rotor windings of the wound rotor induction machine. A fifth order set of differential equations can be written in dq0 coordinates as displayed below. The voltage, current, and flux indices are referred by the direct (*d*) and quadrature (*q*) axes while (*s*) and (*r*) represent the respective stator and rotor quantities [60].

$$V_{ds} = -R_s i_{ds} - \omega_s \psi_{qs} + \dot{\psi}_{ds} \tag{20}$$

$$V_{qs} = -R_s i_{qs} - \omega_s \psi_{ds} + \dot{\psi}_{qs} \tag{21}$$

$$V_{dr} = -R_r i_{dr} - s\omega_s \psi_{qr} + \dot{\psi}_{dr} \tag{22}$$

$$V_{qr} = -R_r i_{qr} - s\omega_s \psi_{dr} + \dot{\psi}_{qr} \tag{23}$$

$$\dot{\omega} = \frac{1}{2H}(T_m - T_e) \tag{24}$$

Of this set of equations 24 describes the motion of the machine. From expressions 20-23 the flux linkages can be derived as shown in 25-28.

$$\psi_{ds} = -(L_s + L_m) i_{ds} - L_m i_{dr} \tag{25}$$

$$\psi_{qs} = -(L_s + L_m) i_{qs} - L_m i_{qr} \tag{26}$$

$$\psi_{dr} = -(L_s + L_m) i_{dr} - L_m i_{ds} \tag{27}$$

$$\psi_{qr} = -(L_s + L_m) i_{qr} - L_m i_{qs} \tag{28}$$

Combining 25-28 and if the stator transients, the flux derivatives in 20-23, are neglected algebraic definitions for voltages may be derived [61].

$$v_{ds} = -R_s i_{ds} + \omega_s((L_s + L_m) i_{qs} + L_m i_{qr}) \tag{29}$$

$$v_{qs} = -R_s i_{qs} - \omega_s((L_s + L_m)i_{ds} + L_m i_{dr}) \tag{30}$$

$$v_{dr} = -R_r i_{qs} + s\omega_s((L_r + L_m)i_{qr} + L_m i_{qs}) \tag{31}$$

$$v_{qr} = -R_r i_{qr} + s\omega_s((L_r + L_m)i_{dr} + L_m i_{ds}) \tag{32}$$

3.1.4 Vector Control

Consider a rotating reference frame rotating in at the same angular velocity (ω_1) as the power grid (ω_s). Revisiting equation set 4-7 and rewriting expression 4 and 5 in the time domain the following stator and rotor expressions may be derived [25].

$$I_s R_s + V_s = -\dot{\psi}_s - j\omega_s \psi_s \tag{33}$$

$$I_r R_r + V_r = -\dot{\psi}_r - j(\omega_s - \omega_r)\psi_r \tag{34}$$

Under the same assumptions above, the d axis of the d-q coordinates is selected to be in line with the stator flux ψ_s. Now, ψ_d remains constant since the stator flux is constant, and thus $\dot{\psi}_d = 0$ and $\psi_q = 0$. These terms can be inputs to the above expressions (33,34) to obtain $V_d = 0$ and $V_q = -\omega_1 \psi_d$. If the stator flux equations are rewritten in terms of I_s then we have

$$I_s = \psi_s - \frac{L_m}{L_s} I_r \qquad \text{where} \quad L_s = L_{sl} + L_m \tag{35}$$

Combining the voltage and flux equations (25-28 and 29-32), one can generate expressions that relate *dq* voltage and current quantities to real and reactive power output of the machine.

$$P = v_{ds} i_{ds} + v_{qs} i_{qs} + v_{dr} i_{dr} + v_{qr} i_{qr} \tag{35}$$

$$Q = v_{qs} i_{ds} - v_{ds} i_{qs} + v_{qr} i_{dr} - v_{dr} i_{qr} \tag{36}$$

Under the assumptions above the stator real and reactive powers may be formulated as follows.

$$P_s = 3/2(V_d I_d + V_q I_q) = 3/2(V_q I_q) = 3/2(\omega_1 \psi_d \frac{L_m}{L_s} I_{qr}) \tag{37}$$

$$Q_s = 3/2(V_d I_d - V_q I_d) = -3/2(V_q I_d) = 3/2(\omega_1 \psi_d (\psi_d - \frac{L_m}{L_s} I_{qr}) \tag{38}$$

It should be noted that the expression for the stator real power is regulated by the I_{qr} component whereas reactive power is controlled by I_{dr}. Now if the rotor flux equations (27 and 28) are used by substitution into 35 for I_s the following can be derived.

$$\psi_r = \frac{L_m}{L_s} \psi_s + (L_r - \frac{L_m^2}{L_s}) I_r \tag{39}$$

If expression (34) is considered in the steady state $\dot{\psi}_r = 0$ and using equation (39) with $L_{sc} = (L_r - \frac{L_m^2}{L_s})$, the rotor voltage equations may be derived as follows.

$$V_{dr} = -R_r I_{dr} + L_{sc}(\omega_1 - \omega_r) I_{qr} \tag{40}$$

$$V_{qr} = -R_r I_{qr} - (\omega_1 - \omega_r (L_{sc} I_{dr} + \frac{L_m}{L_s} \psi_d) \tag{41}$$

From the above equations it should be observed that applying appropriate control to the rotor side converter can produce the necessary voltages to control the stator power. Therefore, the active and reactive power of the DFIG machine may be controlled with the decoupled vector control strategy.

3.1.5 Pitch Control Characteristics

The pitch controller of a DFIG wind turbine is used to regulate the mechanical power extracted from the wind. This strategy becomes useful when mechanical power input to the turbine becomes excessive at high wind speeds. Revisiting expression 12 it is apparent that the mechanical power can be approximated as the cube of the wind speed. Thus a small change in wind speed produces a large change in mechanical power.

In order to help control the turbine input within its design specifications the performance coefficient (*cp*) in 12 must be regulated. It was discussed earlier that the function for *cp* is derived with two variables, (λ, β).

The pitch controller can be represented by the transfer function in a block diagram as shown in Figure 9. The entire subsystem response is comprised of a PI controller that governs the output of the controller, which is then feed into a pitch-actuated servomotor.

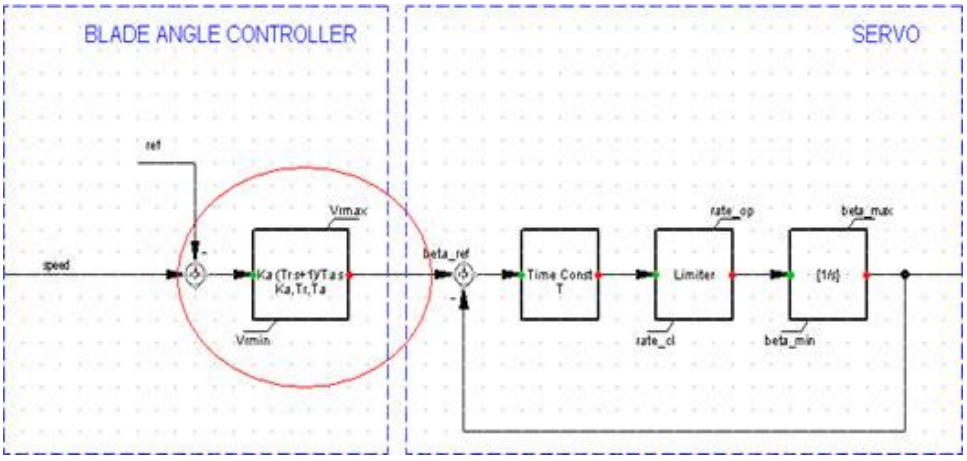

Figure 9. Pitch Controller Block Diagram [30]

The pitch controller modeled in PowerFactory is a generic model that does not represent any individual turbine manufacturer. The model was adjusted to produce a reasonable response as compared with other documented results [59]. Details regarding the design of the pitch controller can be found in numerous literatures [62].

3.2 Dynamic Model Validation

All of the following simulation studies were based on the GE 1.5 xle MW wind turbine. All data regarding the electrical and mechanical machine model can be found in Appendix B.

The default model given in DigSILENT PowerFactory was a 7 MW DFIG wind turbine presumably representative of an off shore machine. In order to appropriately address the effectiveness of adjustments to the default model, a wind speed ramp was applied to the newly configured 1.5 MW machine. This test would demonstrate the accurate operation of the machine by stressing the electrical converter and blade pitch control systems from cut-in to cut-out operation.

3.2.1 Dynamic Model Validation

The below simulations were run to model 400 seconds or approximately 6.5 minutes of a constant linearly increasing wind gust. This wind gust was made to begin at cut-in speed around 4 m/s and increase until cut-out wind speed of 20 m/s. Figure 10 contains eight time simulation plots that contain variables of interest to validate the simulation over the 400 seconds. The output is comprised of 100 wind turbines, which represent the aggregated response of a wind plant and not just one unit.

As the wind ramp gradually increases it can be noticed that the performance coefficient increases from 0.05 at cut-in until around 0.40 at rated wind. At this point the pitch controller activates at around 150 seconds and *cp* begins to exponentially decay until cut-out wind speed. Throughout the entire simulation the total electrical power output of the machine positively increases from around zero. It should also be noted that the rotor power is negative during the sub synchronous operation and positive for super synchronous operation.

And at exactly 1.0 pu shaft speed (synchronous speed) the rotor power is 0. The shaft speed cuts in around 0.75 pu and hits rated speed around 1.25 pu. This corresponds to the +/- 25% speed range designed for this machine. Thus based on the results in Figure 10 it was determined that a wind plant model had been appropriately developed for the scope of this project.

3.3 DFIG Control Enhancements

This section provides information regarding the control structure of the power electronic converter and control enhancements to the default model. The control over the power electronic converter is independent on both the rotor and grid side converters. Information regarding details on the control theory behind this can be found in literature [63].

3.3.1 Electrical PEC Control Structure

The control structure used in the PowerFactory model is depicted in Figure 11. This figure shows three subsection control functions. The "Current" and "Power" subsections were default control loops for the PowerFactory DFIG wind turbine model. The "Protection"

subsection control loop was developed as a part of this work and is meant to be a means of protecting the machine.

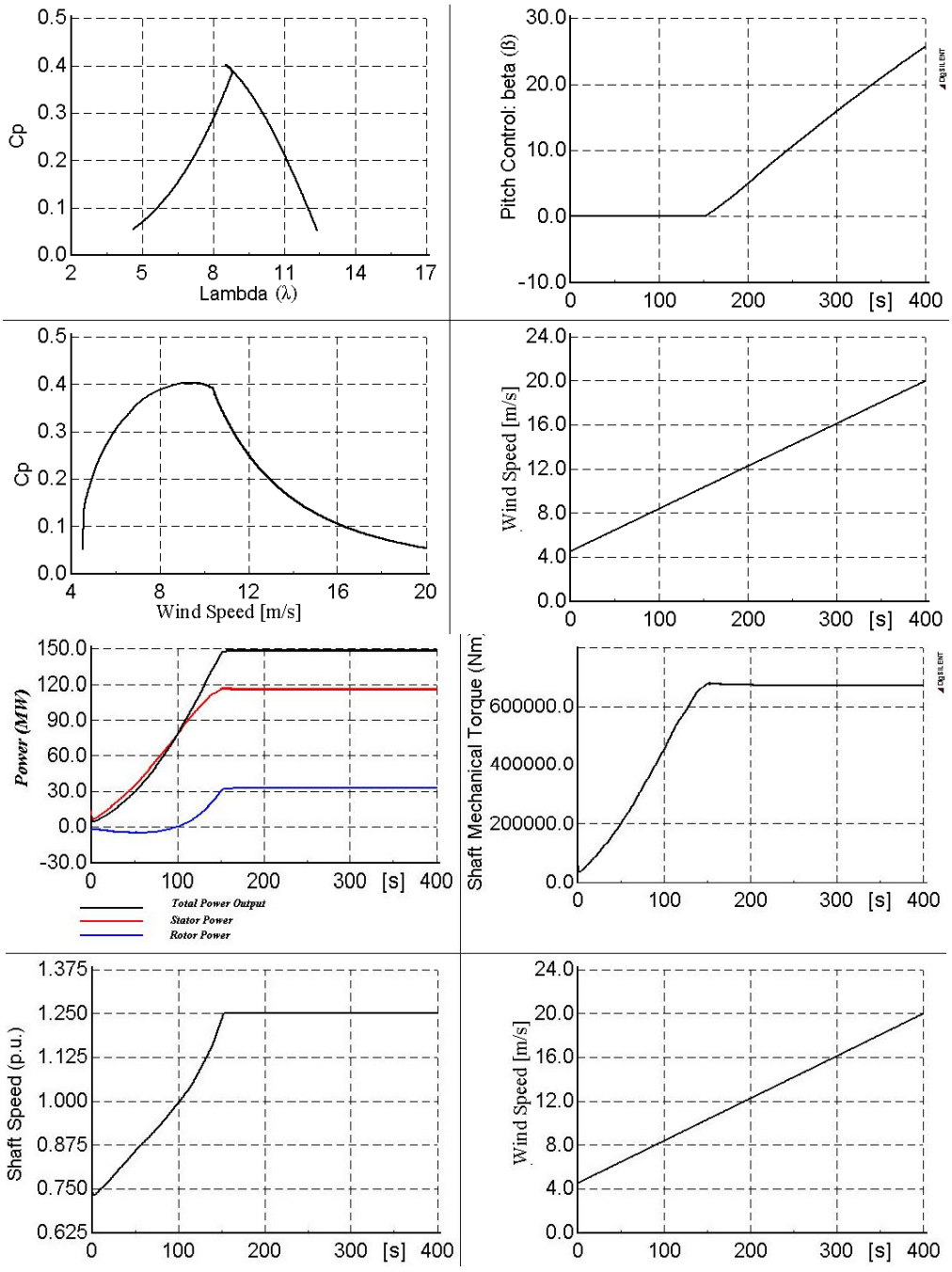

Figure 10. DFIG Dynamic Model Validation

The blocks labeled “DC OV”, “GSC Boost”, and “Re-trip” will be covered in the following section. DC OV is an overvoltage protection circuit and control logic built into the PEC DC link. The GSC Boost allows for the grid side converter to be utilized to provide reactive power when the RSC circuit is in a protected state. And the Re-trip is another hardware circuit and logic to prevent the default DFIG protection circuit from retriggering in the presence of a severe disturbance.

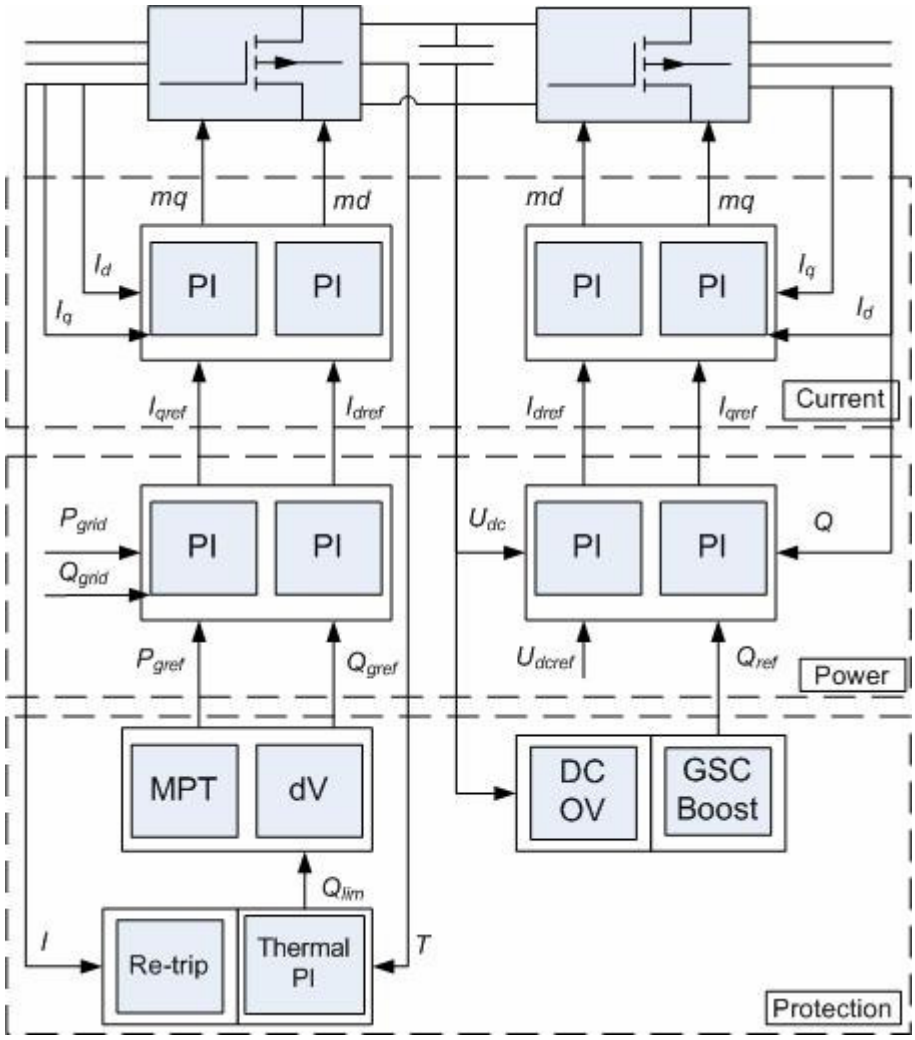

Figure 11. DFIG Power Electronic Control Block Diagram

3.3.2 Controller Development

In this section the development of enhancements made to the DFIG wind turbine control structure will be covered. The control developments are in regards to improvements made to the machine, which increase the likelihood of the plant to contribute to secure operation of the system. In order to test the claimed improvements to the control structure the DFIG wind plant was subject to a severe disturbance as defined by the Federal Energy Regulatory Commission (FERC).

3.3.2.1 Zero Voltage Ride Thorough

As mandated by FERC Order 661-A wind-generating plants are to remain online in the presence of severe voltage disturbances for a defined period and voltage profile [24]. This section will address issues regarding the Post-transition Period that takes affect on all newly installed wind generation from January 1, 2008 to present.

The regulations state that wind plants are to remain on-line during three-phase faults with normal clearing times (4-9 cycles) and single line to ground faults with delayed clearing. The post-fault voltage recovery must return to the pre-fault voltage level. The clearing time requirement for a three-phase fault will be determined by the transmission provider and may not have a clearing time greater than 9 cycles (150 ms). In the event that a fault remains greater than the clearing duration or the post-fault voltage does not recover above the determined value, the wind park may disconnect from the transmission system. Wind generating plants must remain connected during such faults with voltage levels down to 0 volts, as measured at the high side of the POI transformer. Figure 12 summarizes the fault ride through criteria graphically.

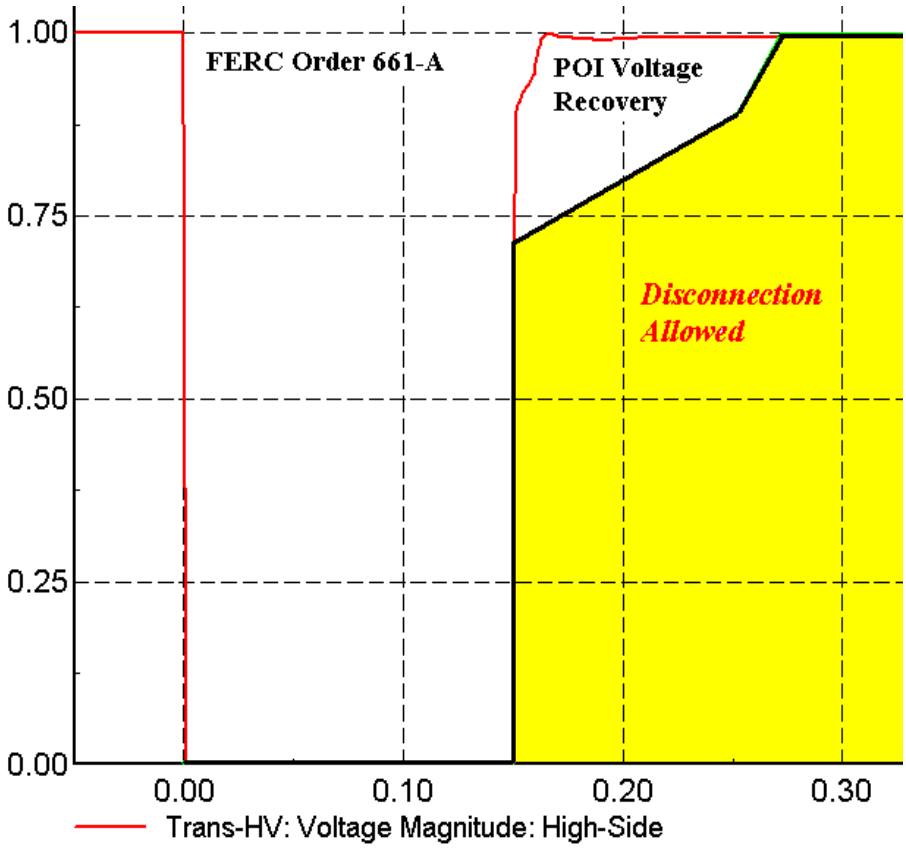

Figure 12. FERC Order 661-A (*Black*) v.s. POI Bus Voltage (*Red*)

All DFIG control enhancements were tested with a 3-phase short circuit at the high side POI using the test system described in Chapter 5. The following sections elaborate on each control enhancement individually and then draw a comparison between the simulation model before and after the control improvement.

3.3.2.1 Protection Response of DFIG Wind Turbines

The main problem inherent in a DFIG machine is the current sensitivity of the IGBTs that make up the power electronics converter [66]. These devices may be subject to damage if converter current limitations are exceeded. Since the RSC of the PEC is connected to the

rotor via slip rings a crowbar circuit may be short circuited in parallel to the rotor windings as depicted in Figure 13.

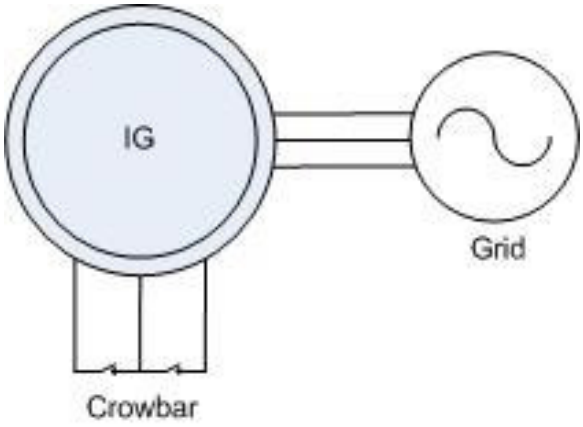

Figure 13. DFIG Crowbar Protection Response Schematic

This action electrically isolates the RSC from damaging transient currents that may be induced into the rotor winds from the stator side of the machine during a disturbance. Figure 14 shows a time dependent simulation of the current through the RSC from pre to post fault. It should be noted that at time 0.0s a short is placed at the high side POI. This action induces large current transients in the RSC just before the RSC protection is triggered. Small transients are observed at 150ms when the protection circuit is cleared and the RSC resynchronizes the machine with the system. The transient currents are thus smaller as the bus voltage has returned to its pre-fault status.

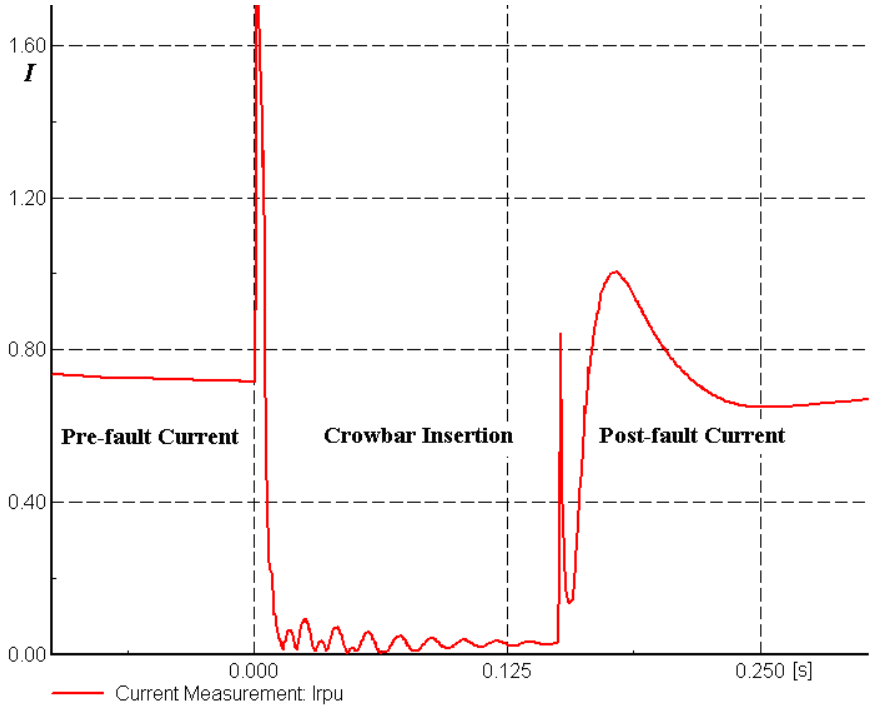

Figure 14. Current Flow in Power Electronics during Crowbar Operation

Although this protects the RSC from potentially damaging currents, it unfortunately disables all excitation and power control that is needed for operation of the DFIG. During the protection period the machine effectively is functioning as a traditional induction generator that becomes an inherent reactive power consumer due to the nature of the machine. Thus, control improvements are presented which are used as an aid to overcome some of these shortcomings discussed during fault conditions in the machine.

3.3.2.2 Grid Side Reactive Power Boosting

During a grid fault where the RSC converter is disconnected from the rotor, as described in the previous section, the machine losses all controllability of real and reactive power. During this protection period the Grid Side Converter may be controlled to provide a

reactive power injection as depicted in Figure 15. Using this strategy effectively utilizes all components of the PEC system and increases the internal bus voltage within the wind farm collector system.

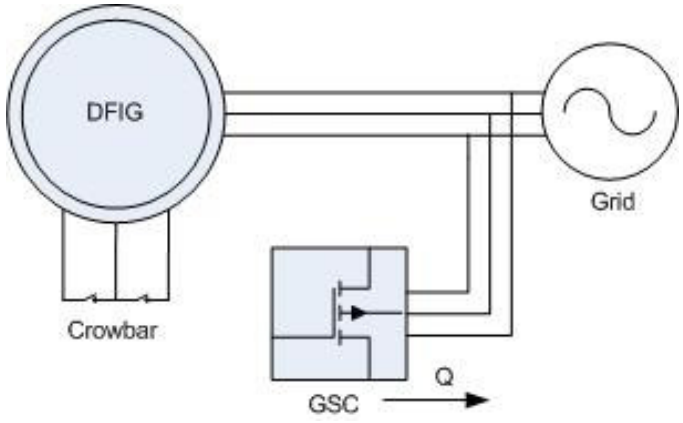

Figure 15. Coordinated Converter Control Schematic during Crowbar Operation

During this period the GSC is effectively functioning as a STATCOM device that may inject or consume a dynamic source of reactive power based on the local system needs [66].

Figure 16 shows the simulation results where the zero-voltage FERC fault criteria were applied and the DFIG protection system triggered as noticed by the diminished collector system terminal voltage. The upper graph in the figure shows the instantaneous response in the GSC reactive injection with and without the GSC reactive power boosting control strategy.

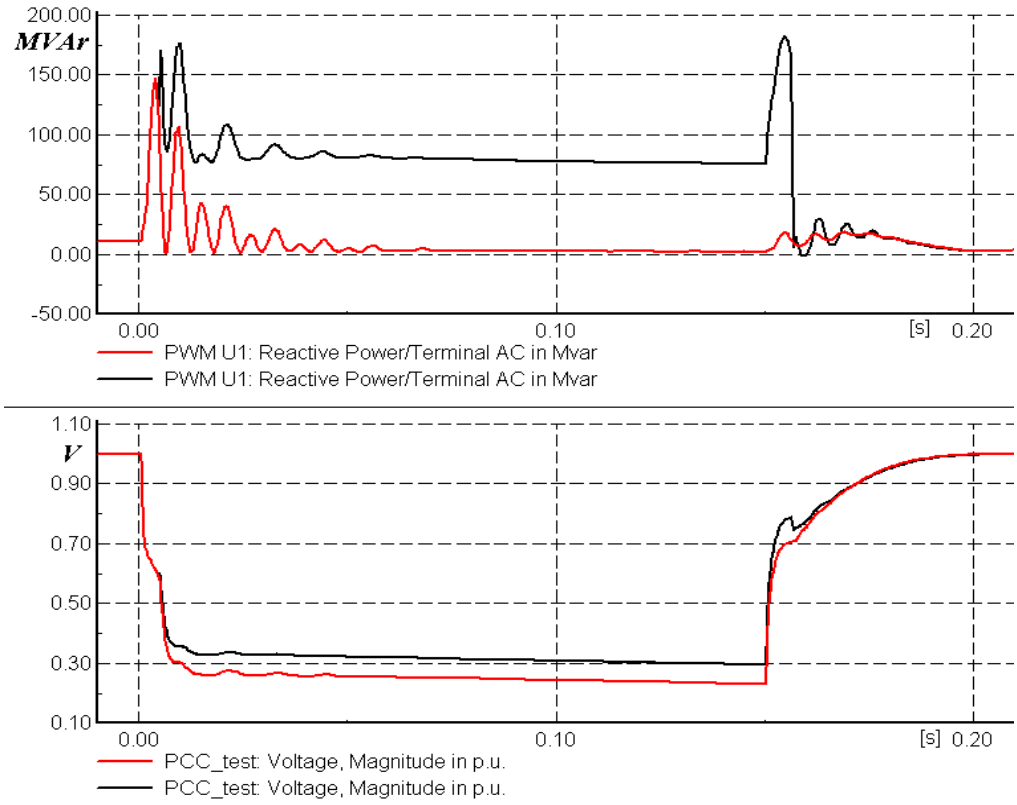

Figure 16. Impact of Grid Side Reactive Boosting with (*black*) and without (*red*) Control

The redlined simulations are using the default DFIG plant model whereas the black-lined results are after the reactive boosting was added. It can be noted that an approximate increase of 7% in the machine terminal voltage was attributed to the GSC boosting during the short-circuited crowbar protection period.

3.3.2.3 Crowbar Protection Re-trip Prevention

As noted earlier the natural response of the DFIG protection upon placing and clearing a fault is induced current transients from the stator to rotor. The transient currents upon fault clearing are much less than the fault initiation, but nonetheless still present in the

rotor and possibly through the RSC. Under certain conditions the transient current produced during the protection clearing has been shown to re-trigger as displayed in Figure 17.

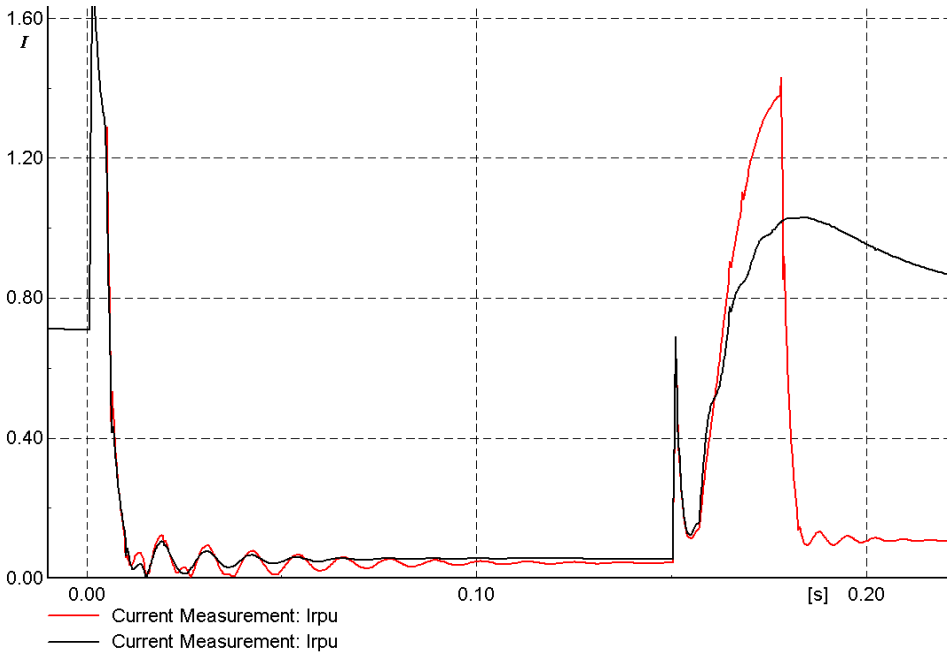

Figure 17. PEC Current with and without Crowbar Re-trip Prevention

The redlined result is the current flow through the RSC before, during, and after the fault without any control modification to the existing DFIG model. If such a scenario were to occur the DFIG plant would remain inoperable for another 150ms until the protection would again resynchronize with the grid. This sustained loss of generation could inevitably repeat itself or have already produced an uncontrolled deterioration to the system during heavily loaded periods.

Either situation may prove devastating; as such the idea of a switched series resistance was mentioned as a potential method to contribute to fault-ride through [67]. Figure 18 shows the schematic representation along with the traditionally included crowbar

protection. That study concluded that hardware costs would out way the benefit of such investment and was not pursued any further.

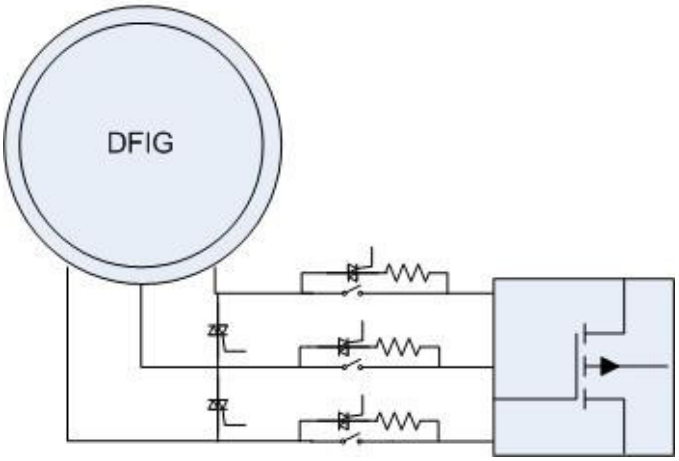

Figure 18. Crowbar Re-trip Prevention Implementation

Instead this investigation delves into the possible effectiveness of this implementation while neglecting the cost burden associated with the equipment. A simulation equivalent of the hardware shown in Figure 18 was programmed into the PowerFactory default model and tested with a short circuit at the POI. The positive effect of reducing the transient rotor currents was observed in the previous Figure 17. It should be noted that upon re-synchronization at 150ms the RSC rotor current (black line) has a substantially reduced magnitude as compared with the original model. Thus the series crowbar implementation complements the already existing parallel crowbar to prevent the re-trip of the machine protection circuit.

3.3.2.4 DC Link Capacitor Over Voltage Mitigation

The DC link capacitor in the PEC circuit is integral for bidirectional power flow between the rotor and grid. Proper voltage levels must be maintained at the DC link in order to effectively control the excitation of the machine and to avoid damage to the capacitor. It has been documented that during certain conditions the DC link may encounter a potentially disastrous scenario when the RSC protection is triggered [64]. Figure 19 shows the voltage magnitude (red-lie) of the link capacitor when the crowbar triggers due to a 3-phase short at the POI for 150ms. It should be noted that nominal DC link voltage is at 1.3 kV and the transient voltage that occurs produces levels of around 1.9 kV.

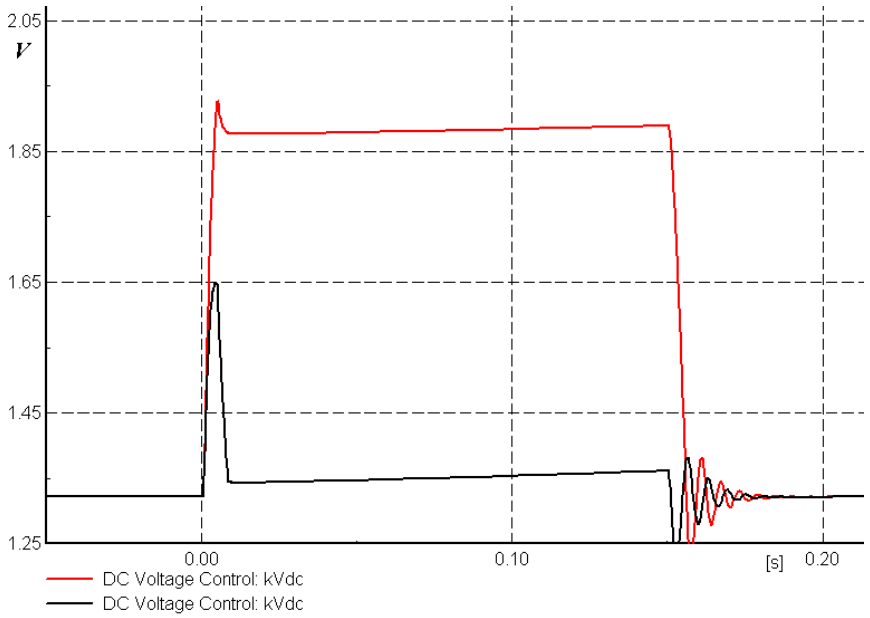

Figure 19. DC Link Capacitor Voltage with and without Chopper Control

This scenario presents itself when the machine is functioning in its sub-synchronous region of operation at high slips. In this regard there is a relatively large amount of energy transfer from the grid through the PEC and to the rotor. When the RSC crowbar trips, the

GSC control cannot instantaneously respond which causes overcharging of the capacitor. This situation can be damaging to PEC circuitry. To mitigate such a problem the chopper circuit shown in Figure 20 has been implemented as found in literature [64].

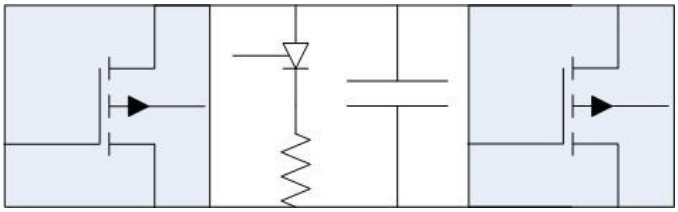

Figure 20. DC Link Chopper Circuit Schematic

The control methodology constantly senses the DC link voltage and activates the chopper circuit at a turn on / off thresholds. The voltage level (black-line) in Figure 19 shows the reduced voltage transient the results from the implemented chopper hardware and control logic using PowerFactory.

CHAPTER 4. VOLTAGE SECURITY ASSESSMENT METHODOLOGY

Reactive power is essential for the stable operation of the power system. It facilitates flow of active power from generation sources to load centers [11]-[13] and maintains bus voltages within prescribed limits [14]. Stable operation of power systems requires the availability of sufficient reactive generation [15]. Figure 21 shows a simplified two-bus power system model that demonstrates the relationship between real and reactive power flows given the machine angles and terminal voltages. Assuming negligible line resistance and transforming the above figure using a Thevenin equivalency the following relations are derived.

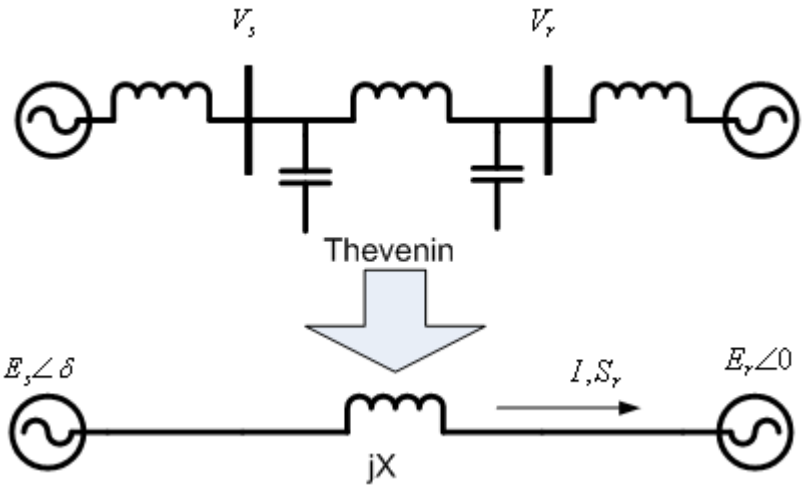

Figure 21. Simplified two bus power system

The sending and receiving end terminal voltages are given by, E_s and E_r with an equivalent line reactance (X) and angle of difference between the machines (δ). From these

definitions the real and reactive power transfer (P_s, P_r) across the line can be define by equations 35 - 37.

$$P_s = P_r = \frac{E_s E_r}{X} \sin \delta \tag{35}$$

$$Q_r = \frac{E_s E_r \cos \delta - E_r^2}{X} \tag{36}$$

$$Q_s = \frac{E_s^2 - E_s E_r \cos \delta}{X} \tag{37}$$

Notice that if the voltage magnitudes are fixed the real power transfer is predominantly governed by the transmission angle (δ). Conversely, the terminal voltages strongly influence the reactive power transfer. Therefore, appropriate reactive capability of machines is essential to maintaining proper voltage levels. Although the above approximations are derived from steady state conditions, the availability of dynamic reactive power sources following a disturbance plays an important role in voltage stability [16], [17].

4.1 Introduction

In this chapter a methodology is outlined which was developed for assessing the security of a power system with high wind penetration. This framework is a two-stage process that first determines the maximum wind penetration allowable into a given location from static analysis. The second stage of the process considers the power flow solution and analytical results from the first stage in order to perform dynamic simulation of the system. The dynamics part of the methodology assesses the integrity of the system following a select list of critical contingencies.

The two-part procedure uses industry grade reliability standards as a metric for evaluation of system health. Following the completion of the outlined methodology, it can be determined if the proposed wind penetration levels are valid based on the voltage security assessment.

4.1.1 Static Security Assessment for High Wind Penetration

A Voltage Security Assessment (VSA) was developed using criteria set forth by the Western Electricity Coordination Council (WECC) and North American Electric Reliability Corporation (NERC) [65]. The VSA methodology integrates a static security standard that uniquely aids in identifying system deficiencies when large wind penetration is present. Dynamic simulations are then run to validate that the proposed penetration level will be appropriate for the power system. A detailed description of how to perform the VSA will be introduced next.

4.1.1.1 Methodology Description

The VSA is formulated around a steady state power flow solution that is deemed secure by WECC standards. This process is the heart of the VSA, as the dynamics are only to validate an appropriate level of wind penetration. The steady state analysis is used to identify the levels to be tested. The following descriptions will elaborate on the VSA flow chart depicted in Figure 22.

1. A matrix case list of penetration levels and park outputs must be defined which will be tested on the base case system. Table 2 defines 16 possible combinations of base case scenarios that could potentially be selected. There are four

penetration levels (15%-30%) containing four plant outputs (0%-100%) that correspond from cut-in to cutout wind speeds. All output levels should be run for the lowest penetration level being tested before moving on to the next penetration level.

Table 2. Base Case Scenario List

Penetration Level / *Plant Output*	***15%***	***20 %***	***25%***	***30%***
0%	1	2	3	4
33%	5	6	7	8
66%	9	10	11	12
100%	13	14	15	16

2. For each of the above 16 scenarios a list of critical contingencies is defined through a screening and ranking procedure [68]. For the purpose of this VSA only voltage levels are considered as a criterion for selecting the most crucial outages. All generator and line outages were considered as possible n-1 contingencies. To screen the n-1 outage, the base case bus voltages were compared against the respective bus voltage in each n-1 scenario and ranked in order of magnitude. A select number of the largest voltage differences were used for each of the 16 case scenarios.

3. PV analysis is performed using the identified list of critical contingencies [68]. At each incremental increase in load all critical contingences are run and all performance metrics are checked against the respective criteria limits. The PV analysis will proceed until a violation is reached. This study considered proportionally increasing the entire system load although a single study area may be of interest for large systems.

4. Stopping criteria for the PV analysis is based on a combination of limits including WECC steady state voltage criteria and a satisfactory power transfer margin of the system. A transfer margin should be determined based on engineering judgment and as such, the base case scenario without wind was used as the metric of comparison.

5. After completing the scenarios for all plant output levels and all given penetration levels, shunt placements can strategically be determined. For each PV analysis of scenarios, a certain load level was determined. The load level increase was stopped due to voltage violation at one bus. This bus is then deemed the critical bus and each case will contain one. Again using engineering judgment or given a repeated critical bus based from all scenarios, shunt compensation of a selected amount can then be applied.

6. When the PV analysis for one case is completed a suitable transfer margin and voltage levels are assumed to be established. Thus the next penetration and

output case file from the initial case list matrix should be loaded and run. This procedure should be repeated until all cases have tried with the VSA method.

7. The maximum penetration level can then be identified for the steady state. This penetration level is determined based on a suitable transfer margin from each of the tested output levels for a given tested penetration level. Here is a sample example. For a tested penetration level of 25%, transfer margins of 12%, 25%, 28%, and 20% were found from each of the four plant output percentages. Therefore, if an acceptable system transfer margin of 10% is allowable, then a 25% penetration level is acceptable. But if a transfer margin of 15% is necessary, 25% wind penetration would no be appropriate since one of the four transfer margins was only 12%.

8. Lastly, dynamic simulation of several critical faults should be run on the system for various wind plant output levels. This can validate whether the system is stable at the now installed penetration level.

4.2 Dynamic Validation of Wind Penetration Level

Once a penetration level is defined as secure in the steady state, then dynamic simulation of those given load and generation conditions can be validated. The dynamic security aspect incorporates the results from the static assessment and therefore may validate

whether the steady state wind penetration level is acceptable. Thus severe or critical contingencies are identified and tested with appropriate simulation models.

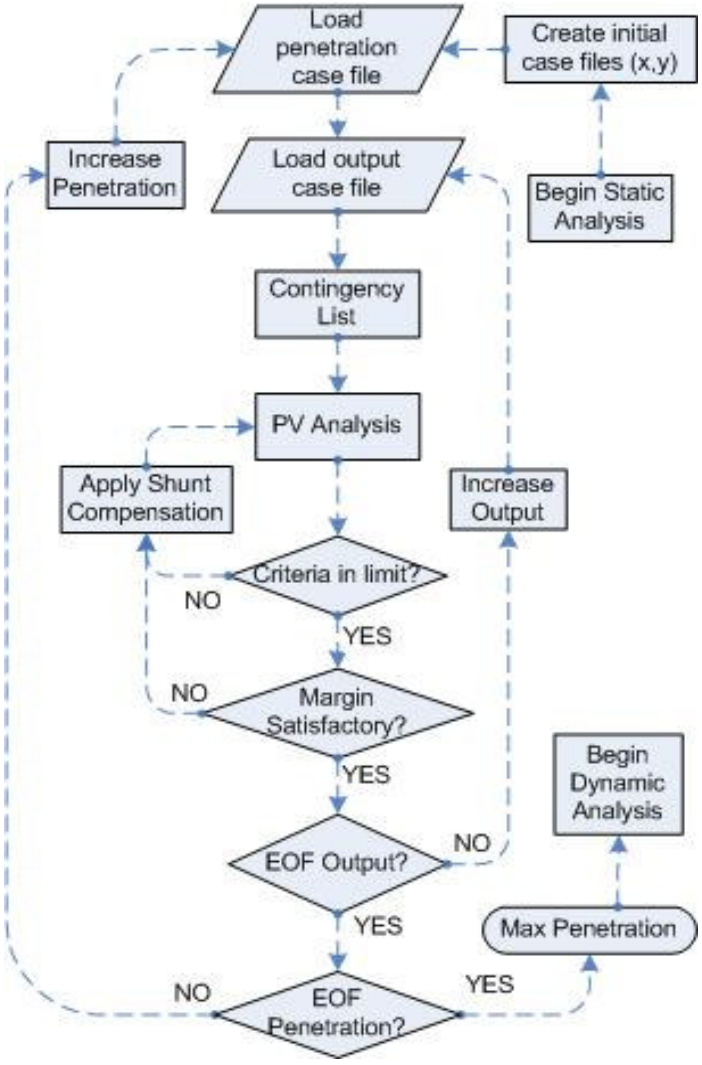

Figure 22. Voltage Security Assessment Flow Chart for High Wind Penetration

CHAPTER 5. DISCUSSION AND ANALYSIS OF RESULTS

This chapter consists of a two-part discussion involving the analysis of the results from implementing the VSA on a test power system. Section 5.1 covers the static results of the Voltage Security Assessment and 5.2 details the dynamic validation of the selected penetration level from the VSA.

The Voltage Security Assessment methodology was performed using the VSAT software program found in the DSA Tools package developed by PowerTech [68]. The dynamic validation of the chosen wind penetration level was performed in PowerFactory software simulation package developed by DIgSILENT.

5.1 Power System Description

A sample power network available in the PSS/E software was imported into VSAT and PowerFactory for system analysis. The original network consists of 6 conventional machines and 26 buses. The total load was modified to 3035 MW and 1230 MVAr with 305 MW of motor load that has been distributed between buses 3005, 153, 203. Refer to figure 23 for the schematic of the network. Shunt compensation (950 MVAr sum) is located at various buses throughout the system with a large 600 MVAr reactor at bus 151. The transmission voltages range from 230 – 500kV and the line parameters have been modified to reflect appropriate transmission distances [11].

In the base case the majority of generation is concentrated in the Northern region of the grid. The load centers are located in the South and Southeast portion of the system with major concentration at buse s 154 and 206. The Southwest part of the network contains low

load and low transmission capacity. Typical high wind regions have these characteristics and hence it is assumed a potential site for large-scale wind facilities [43].

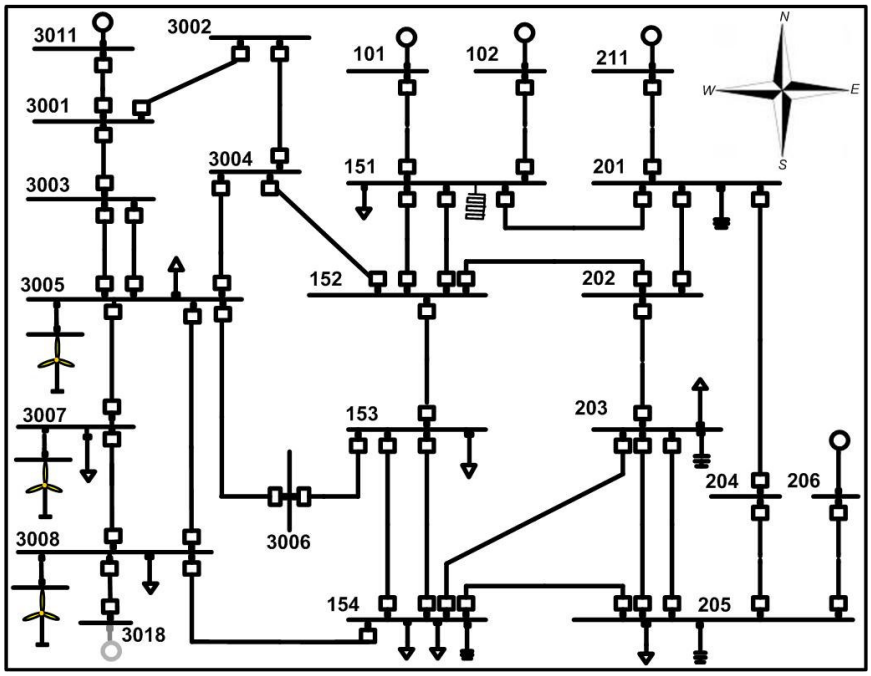

Figure 23. **Simulated Power System with Wind Park Interconnection at Bus 3008**

Since one of the underlying themes of this research is to address the implementation of large DFIG penetration levels, unit 3018 has been taken off line. Installed in place of this unit are 3 DFIG wind facilities strategically placed at buses 3005/ 7/ 8. The replacement of this unit was to simulate isolated wind generation that would emphasize the impact of high DFIG penetration on system performance. To facilitate the transfer of energy from these high wind regions to the load centers the lines (3008 – 154), (3005 – 3007), and (3007 – 3008) are upgraded to have sufficient transmission capacity.

5.1.1 Penetration Level Characteristics

Additionally, to analyze the impact of increased DFIG wind penetration, various penetration levels at 15, 20, 25, and 30% are simulated. In this study wind penetration is defined as the total capacity of wind generation compared to the total load.

$$Penetration \quad Level = \frac{\sum Installed \quad wind \quad capacity}{\sum Load} \tag{38}$$

5.1.2 Transfer Margin with Extended Reactive Capability

The transfer margin (TM) of a system was defined by as the percentage increase in load (MW) beyond the base case found in the PV analysis. Equation 39 was used to define the transfer margin of a system for this study.

$$TM = \frac{MW_{PV} - MW_{base case}}{MW_{base case}} \tag{39}$$

5.2 Static Analysis Results

The results from the VSA are presented in the sequence that follows the flow from the chart in Figure 22 from Chapter 4. The VSAs inner iterative "Shunt Compensation" loop was entered on three occasions. This method strategically placed compensation that allowed for an increase in the power transfer margin and thus an overall increase in wind penetration.

The base case list of scenarios was compiled based on the MW injections of the wind park outputs as shown in Table 3. Although, the MW injections are 0 for each penetration

level in the 0% plant output case, this is does not mean that the power transfer of the system will be the same for each penetration.

Table 3. MW injections for given wind penetration and park output

Penetration Level / *Plant Output*	***15%***	***20 %***	***25%***	***30%***
0%	0	0	0	0
33%	115	155	190	230
66%	230	310	385	470
100%	350	470	585	700

Since the wind parks are modeled after modeled after the GE 1.5 MW wind turbine, reactive capability is assumed even when the plant is not producing real power [68]. It is assumed that reactive production is approximately 30% of 1.5MW due to a partial scale PEC converter. This additional reactive capability can be drastically noticed when comparing the power transfer margin for 15, 20, and 25% penetration levels in the 0% output case in Figure 24.

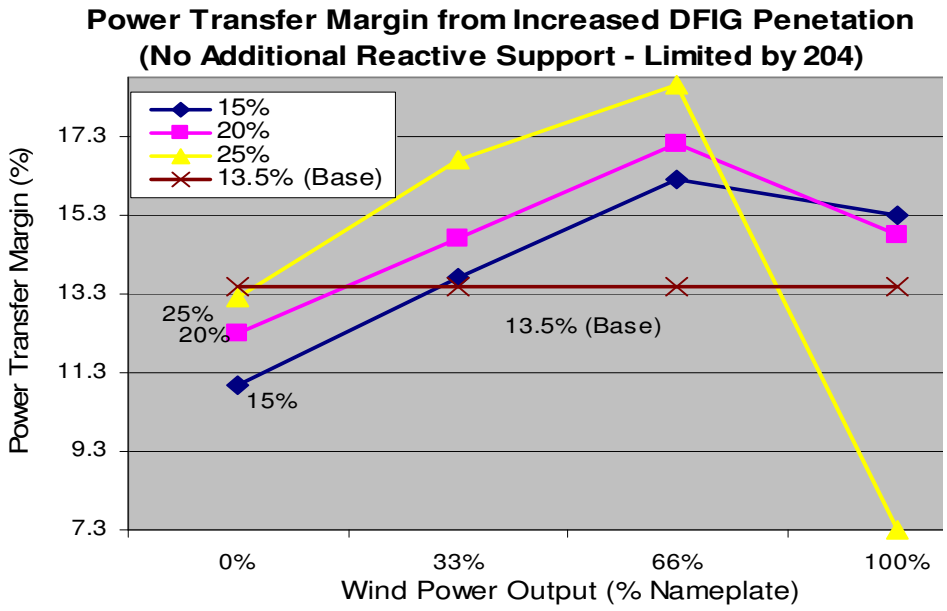

Figure 24. Power Transfer Margin from Increased Plant Output with No Reactive Compensation

The first round of the VSA was tested with only 15, 20, and 25% penetration levels and 30% was initially neglected. This is due to a limited power transfer margin as can be noticed at 25% penetration with 100% plant output. Therefore, 30% penetration was not investigated further for the base case with no shunt compensation.

The base power transfer (or scenario without wind) was used as a metric of comparison for all wind penetration cases. Table 4 shows the numerical results of Figure 24. The table shows that the power transfer margin was lower at 0% output production for both 15 and 20% penetration levels as compared with the 13.5% base scenario. In contrast 25% penetration was severely limited at 100% plant output. The identified contingency that breached the security constraints was the loss of unit 206 (contingency A30 or B3).

Table 4. Power Transfer Margin at Different Penetration Levels with No Reactive Support

Penetration Level / *Plant Output*	***15%***	***20 %***	***25%***
0%	11	12.3	13.2
33%	13.7	14.7	16.7
66%	16.2	17.1	18.6
100%	15.3	14.8	7.3

Following the VSA methodology, an SVC of 50 MVAr reactive support of was located at bus 204 as an aid to increase the power transfer margin. The first round of the VSA provided valuable information regarding the current systems ability to handle an increase in DFIG wind penetration. It is obvious that any wind penetration amount between 15-25% would not be feasible from a reliability stand point as the base case conventional system has a 13.5% power transfer margin. Given the new reactive compensation placed in the system the second iteration of the VSA will be elaborated on.

After the additional shunt was placed at bus 204 substantial overall increase in power transfer for all wind penetration levels (15-25%) was noticed. At a 15-25% penetration levels, bus 204 again becomes the limiting factor at 0% output with the loss of unit 206. Therefore, additional shunt compensation may need to be installed at 204 before reaching higher transfer margins. Figure 25 graphically depicts the transfer margins for 15-25% penetration against the base case (0% wind penetration) scenario. The additional of 50 MVAR at bus 204 allows for around a low of 14% and high of 19% power transfer for a 20%

wind penetration level scenario. At this level an increase in wind penetration allows for a higher transfer than the base scenario.

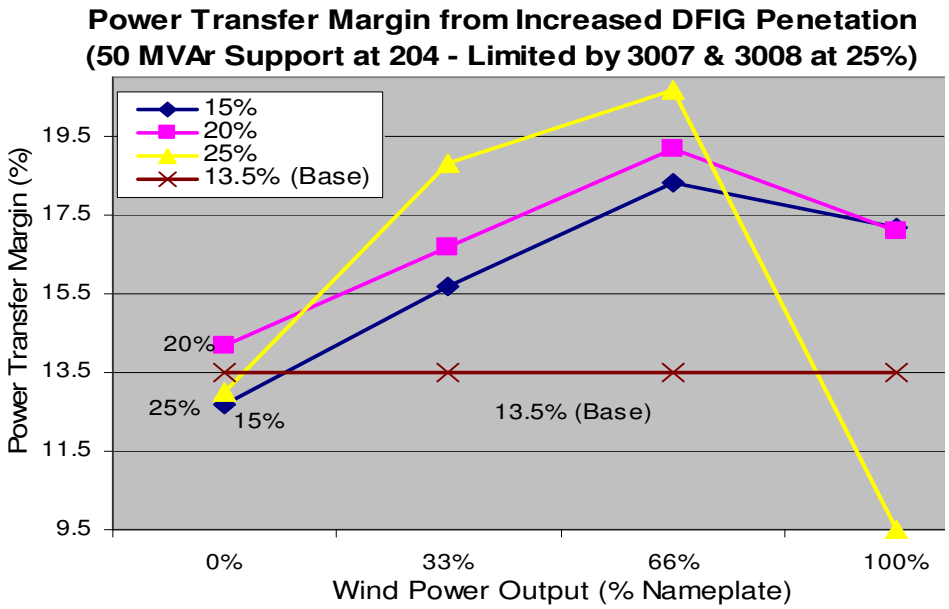

Figure 25. Power Transfer Margin from Increased Plant Output and 50 MVAr Support at 204

It should be noticed that a 25% DFIG penetration level is limited by at both 0% and 100% park output paired against the base scenario. The limiting buses are found by the VSA to be 3007 and 3008 which coincidently are in the location of the installed wind facility Following the VSA procedure another 50 MVAr of shunt compensation was installed. This time the location of the installation was at the high side of the DFIG POI at bus 3008. Since the system was observed to handle 20% wind penetration reliably above the base case, the 15% penetration level was not considered in the next round of VSA simulations. Table 5 marks the numeric results from the above Figure 25.

Table 5. Power Transfer Margin at Different Penetration Levels (50 MVAr at 204)

Penetration Level / *Plant Output*	*15%*	*20 %*	*25%*
0%	12.7	14.2	13.0
33%	15.7	16.7	18.8
66%	18.3	19.2	20.7
100%	17.2	17.1	9.5

Again, after following the VSA with the placement of 50 MVAR at bus 3008, simulations for penetration levels of 20, 25, and 30% penetration were conducted. At this point after running the simulations with input from the VSA it can be concluded from Figure 26 that the total allowable DFIG wind potential in this system is at least 20% and no more than 25% penetration. This is based on the assumption that no other forms of reactive support are investigated. Using engineering judgment, it was concluded that a limit of 30% DFIG wind penetration in the test system was sufficient. Figure 26 shows that penetration levels in the range of 20-25% have a power transfer margin equal to or greater than the base case margin of 13.5%. Since the VSA has provided that all n-1 voltage levels are satisfactory for these load increases and the 20-25% penetration transfer margins are equal to or above the 13.5%, these conclusions are deemed valid.

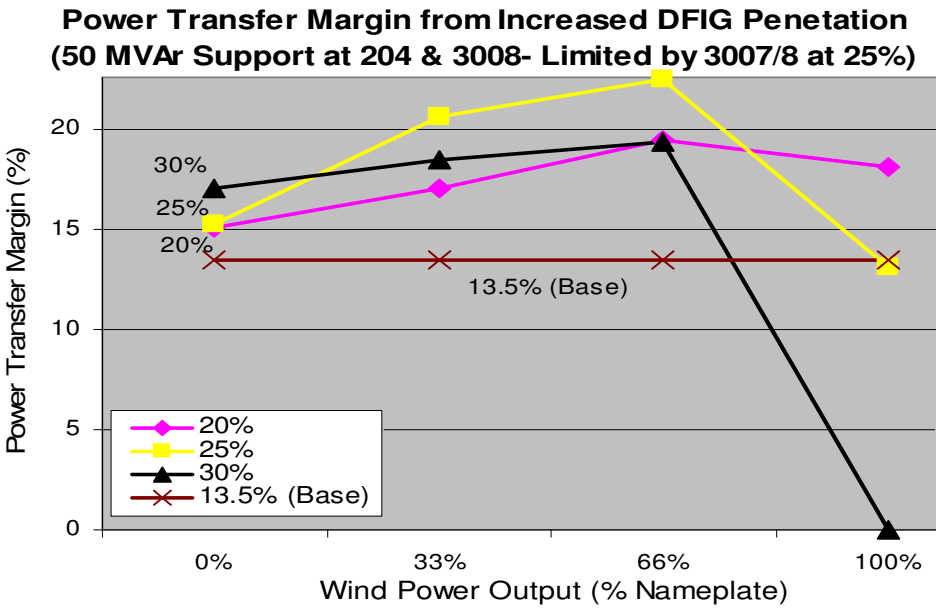

Figure 26. Power Transfer Margin from Increased Plant Output 50 MVAr support at 204 & 3008

It is very interesting to decipher what caused a 0% transfer at 100% plant output from 30% DFIG penetration. In this case the poweflow solution would not converge and was determined to be unstable. This was investigated further and a conclusion was reached that the reactive capability necessary to transfer all 700 MW from bus 3008 into the system was not sufficient. Therefore a larger source of reactive capability would be needed in the local vicinity in order to ship this amount of power out of the wind corridor. A possible solution that was not investigated would be to utilize unit 3018 that was taken off line as a source of reactive compensation. Table 6 shows the numeric results from this last iteration of the Voltage Security Assessment for large-scale wind production facilities.

Table 6. Power Transfer Margin at Different Penetration Levels (50 MVAr at 204 and 3008)

Penetration Level / *Plant Output*	***20%***	***25 %***	***30%***
0%	15.1	15.3	17.1
33%	17.1	20.6	18.5
66%	19.5	22.5	19.4
100%	18.1	13.1	Unstable

5.3 Dynamic Analysis Results

This section provides information regarding the results of dynamic simulations run on the test power system for a 20% DFIG wind penetration level. These simulations are to validate the installation of a large amount of DFIG units put in place of unit 3018 as found in the VSA methodology. These simulations not only test the validity of a 25% wind penetration, but also the performance of utilizing an extended reactive capability curve as described in the earlier Chapter 1. Section 5.3.1 explains the details behind the reactive capability comparison for the DFIG plants.

5.3.1 Voltage Control Application

There are two voltage control strategies that are implemented to demonstrate a comparison between DFIG park responses on system performance. The first strategy utilizes

the +/- 0.95 power factor regulation set forth by FERC order 661-A, where the reactive limits are defined by the parks real output [24].

$$\left|Q_{\max}\right| = P_{output} \tan(\cos^{-1}(0.95)) \tag{40}$$

The second strategy utilizes the reactive capability that is detailed in the developed capability curve in figure 6. Both schemes use a proportional-integral (PI) controller that regulates the POI voltage as outlined in figure 27 [31].

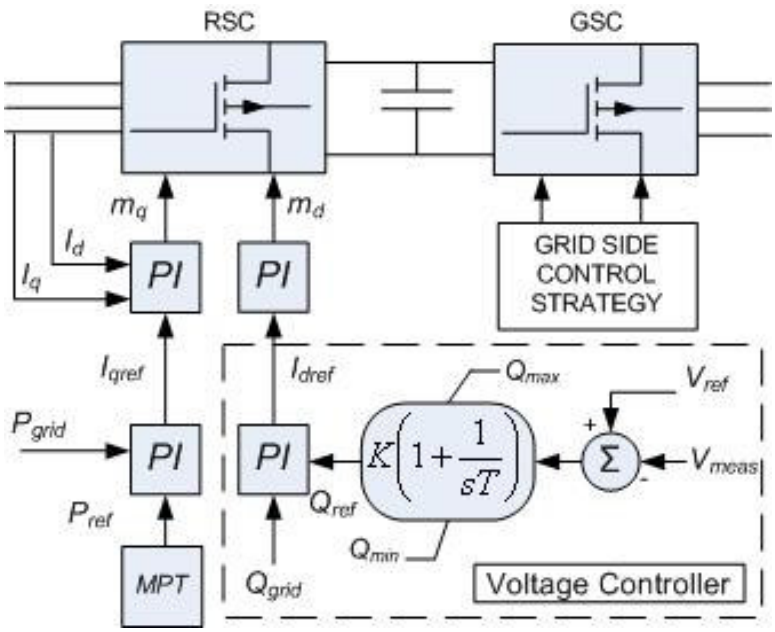

Figure 27. DFIG Wind Plant Voltage Controller Schematic

The inputs to the controller are the set point voltage (V_{ref}) and the voltage measurement (V_{meas}) at the POI. The error signal between the voltages is used by the controller to compute the reactive power set point (Q_{ref}) of the DFIG. The range of control

depends on the reactive limits of the DFIG ($Q_{max,}$ Q_{min}). This voltage controller was incorporated into the existing DFIG control model available in PowerFactory. The controller design was developed using DIgSILENT Simulation Language (DSL) to compare the dynamic response of the strategies.

The main difference between the control strategies is the reactive power limitations ($Q_{max,}$ Q_{min}) placed on the controller for a given real output. This variation in the limits will test the system response between the extended reactive limits of the capability curve over the regulated power factor limitations.

5.3.2 Dynamic Scenario Setup

At each penetration level the total wind generation is simulated at 2, 15, 50, and 100% output in order to consider various production conditions from cut-in to cut-out wind speeds. Since wind is not a constant resource this study aims to capture the effect of wind variability on system reliability.

At 2% park output it is considered that the wind units have just cut-in and the real power output is at a minimum. When employing the capability curve, the reactive limits of the machines are the greatest at this output as compared the other output levels studied. As wind speeds increase the parks real output increases and consequently the reactive capability of the DFIG park reduces. In contrast, the FERC regulation allows wind units to increase their reactive capability as the real output is increased. Again referring to figure 6, at 100% real output the leading reactive capability of both strategies is approximately equal.

Dynamic system data includes standard IEEE exciter and governor models imported from PSS/E for all synchronous machines. All motor loads are represented by standard induction machine models.

5.3.2 System Performance Validation

Given the static results gathered from the VSA analysis, dynamic simulation was carried out in DIgSILENT PowerFactory to analyze the transient response of the test system. Simulations were performed using RMS values (3rd order simulation models) that capture the electromechanical transients [29]. The inherent DFIG model in PowerFactory was modified to incorporate the designed voltage controller and derived converter ratings from the previous sections. The parameters of the modified DFIG model are given in Appendix B.

Four power output scenarios are tested in order to assess the impact of the reactive control strategies with a high level of DFIG wind penetration. Wind park outputs of 2% (cut-in wind speed), 15%, 50%, and 100% generation are simulated on the previously described power system with a 20% penetration level of distributed DFIG wind generation.

The area around bus 3001 was identified as a critical fault location. A 3-phase short circuit was applied at this bus for a duration of 0.14 seconds to compare the responses between the voltage control strategies. It was determined in the VSA study that as penetration levels increase the reactive capability of the DFIG parks was insufficient for secure system operation. Hence, additional switched shunt capacitor banks of 150 MVAr were placed at buses 3005 and 3008 to ensure an accurate comparison of both strategies.

For each control strategy the parks were initialized to 0.95 leading power factor. This ensured that pre-fault conditions of all machines are identical in each scenario for both

control strategies. Before each simulation is performed the corresponding reactive limits are placed on the controller shown in Figure 27. As such, the (P, Q) coordinates are taken from the reactive power curve in Figure 6 and the regulated power factor limits are computed from (40) for the respective real outputs. The upper and lower reactive bounds, Q_{max} and Q_{max} in per units, are the limits for the voltage controller. The controller parameters are K=1 and T=0.001.

The following plots (Figures 28-31) detail the DFIG wind park responses to the disturbance near the fault at park 3005 and further away at park 3008. Each figure contains two sets of plots to compare the voltage control strategies. The three quantities of comparison are: voltage at load bus 153, reactive power output, and rotor current magnitudes through the PEC.

Bus 153 has been selected for monitoring its voltage performance due to the fact that it contains 42% of the system motor load. This bus voltage will be used as a metric of comparison between the voltage control strategies. Other quantities of interest are the total park reactive injections and rotor currents, which are integral in determining whether the wind plants electrical control is disabled.

The power electronic converter protection limitations were strictly taken into account with an over current setting of 600A (1.27 p.u.) given the 470A nominal current magnitude found from the converter sizing. Once triggered a resistive crowbar short-circuits the rotor windings for 0.15 seconds.

5.3.2.1 Scenario 1: 2% Output (Cut-in speed)

This scenario tests the system response for minimum wind levels when the turbines have just cut-in (4 m/s). The Q limits (p.u.) used in the controller based on the capability curve (CC) were (0.72,-0.92) and (0.0, 0.0) using the restricted power factor (RPF) mode. It can be observed from the bus 153 voltage in figure 28 that with the RPF control scheme the system voltages are unable to recover post fault. In both strategies the PEC crowbar protection does not activate thus allows reactive injections through the fault. At fault clearance in the CC case the DFIG plants are able to dynamically compensate for the reactive burden placed on the synchronous generators by the induction motors. Thus, utilizing the extended reactive capability in the CC case stabilizes the system and prevents collapse.

5.3.2.2 Scenario 2: 15% Output

At 15% park output the corresponding Q limits for this study are (0.70, -0.90) for the CC case and (0.08, -0.08) for the RPF case. The PEC protection again does not activate at the fault initiation and over loading of the converters does not occur during the transient. Observing the bus voltage plots in figure 29 demonstrate that the CC control case provides enhanced post fault clearance voltage response. This is noticed in the reduced voltage overshoot as well as reduced ripple magnitudes. The improved post fault system response in the CC case is mainly attributed to the increased reactive consumption at wind plant 3005 as viewed in the reactive plots.

5.3.2.3 Scenario 3: 50% Output

At 50% park output the corresponding Q limits for this study are (0.60, -0.85) for the CC case and (0.18, -0.18) for the RPF case. The PEC protection trips at park 3005 at the fault initialization of the RPF case. This is depicted in the current plots of figure 30. Again the increased reactive consumption is very dominant in the CC case.

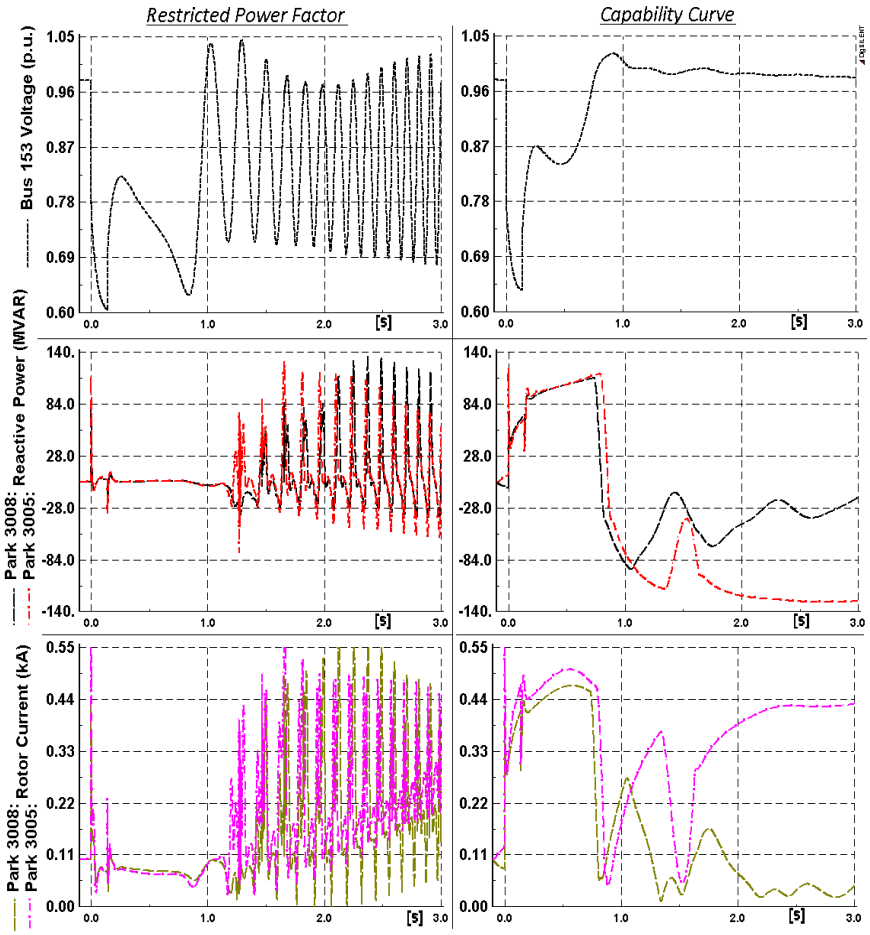

Figure 28. Comparison of bus 153 voltage (p.u.), reactive power (MVAr) (parks: 3008/5 – red/black), and rotor current (kA) (parks: 3008/5 – pink/brown) from 20% penetration at cut-in speed with RPF (left) and with CC (right) control

5.3.2.4 Scenario 4: 100% Output

The final study considers wind plant outputs to be at maximum capacity. The reactive limits placed on this study are (0.36, -0.69) for the CC and (0.34, -0.34) for the RPF modes of operation. It can be observed from the plots in figure 31, as the active power output of a park increases likewise does the current magnitude.

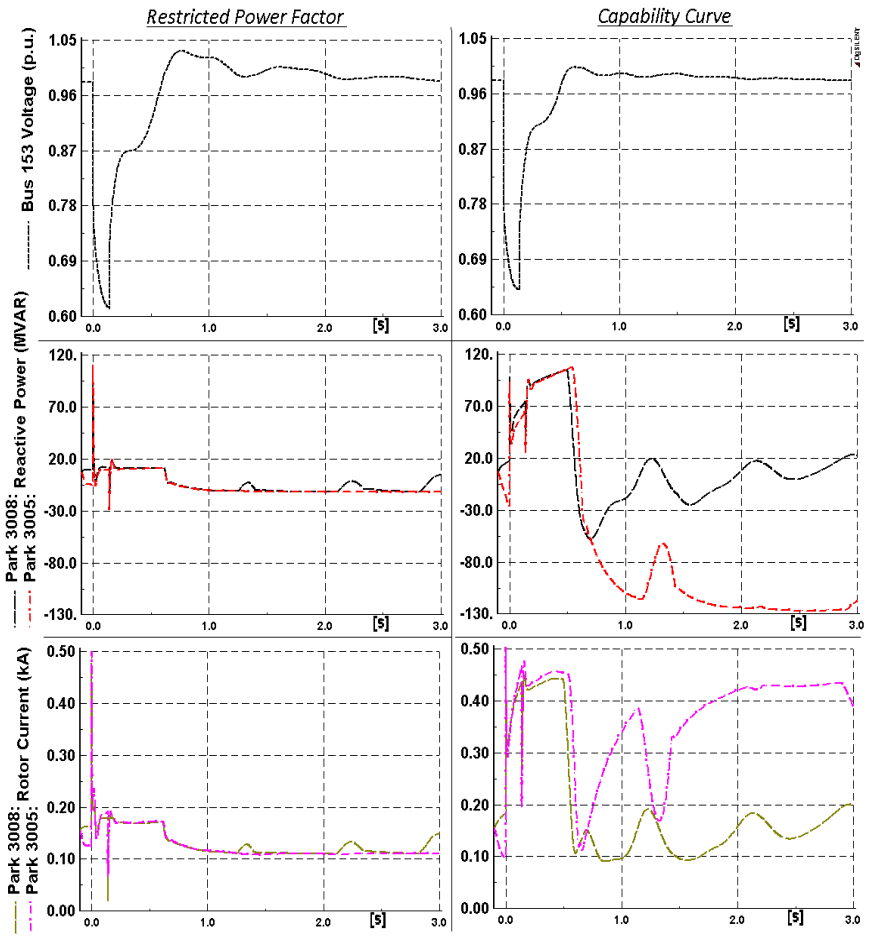

Figure 29. Comparison of bus 153 voltage (p.u.), reactive power (MVAr) (parks: 3008/5 – red/black), and rotor current (kA) (parks: 3008/5 – pink/brown) from 20% penetration at 15% output with RPF (left) and with CC (right) control

The near nominal current at the initiation of the fault leads to tripping of the all wind parks (3005/7/8) PEC in both cases. At 0.15 seconds into both simulations the rotor protection clears, but due to large current transients the protection retriggers and none of the wind plants can regain power controllability until 0.30 seconds after the fault. In both cases the leading reactive limits are very similar hence the near identical reactive injections from wind farm 3008 and the voltage recovery at bus 153.

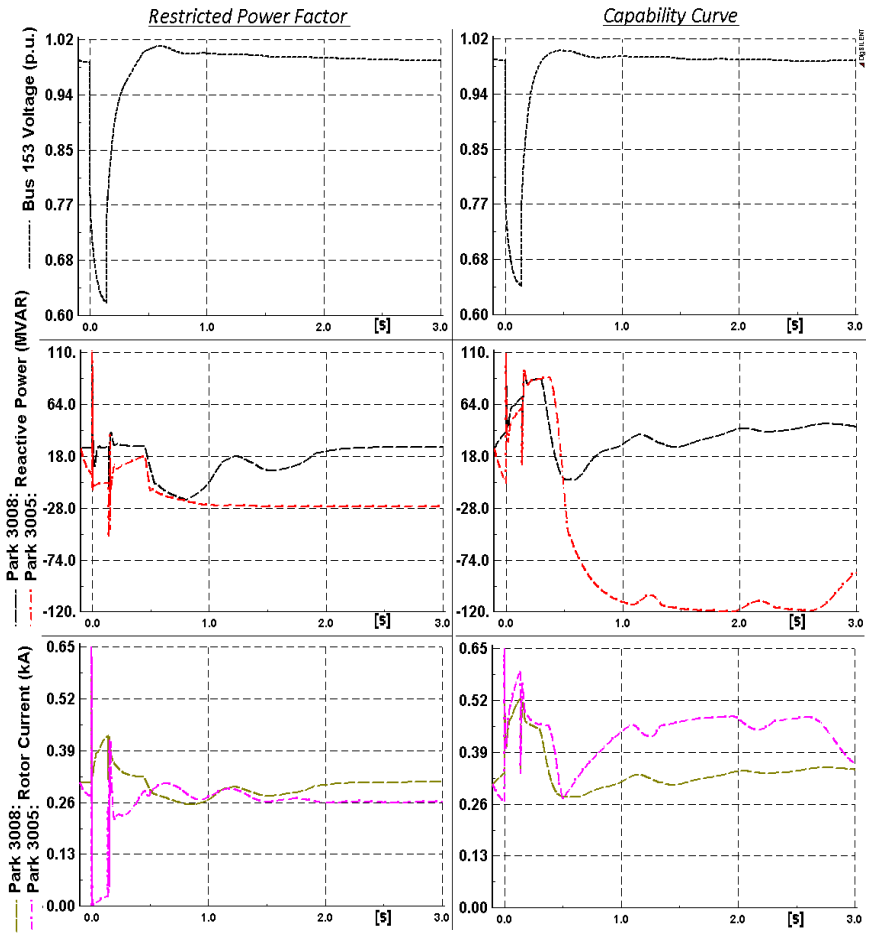

Figure 30. Comparison of bus 153 voltage (p.u.), reactive power (MVAr) (parks: 3008/5 – red/black), and rotor current (kA) (parks: 3008/5 – pink/brown) from 20% penetration at 50% output with RPF (left) and with CC (right) control

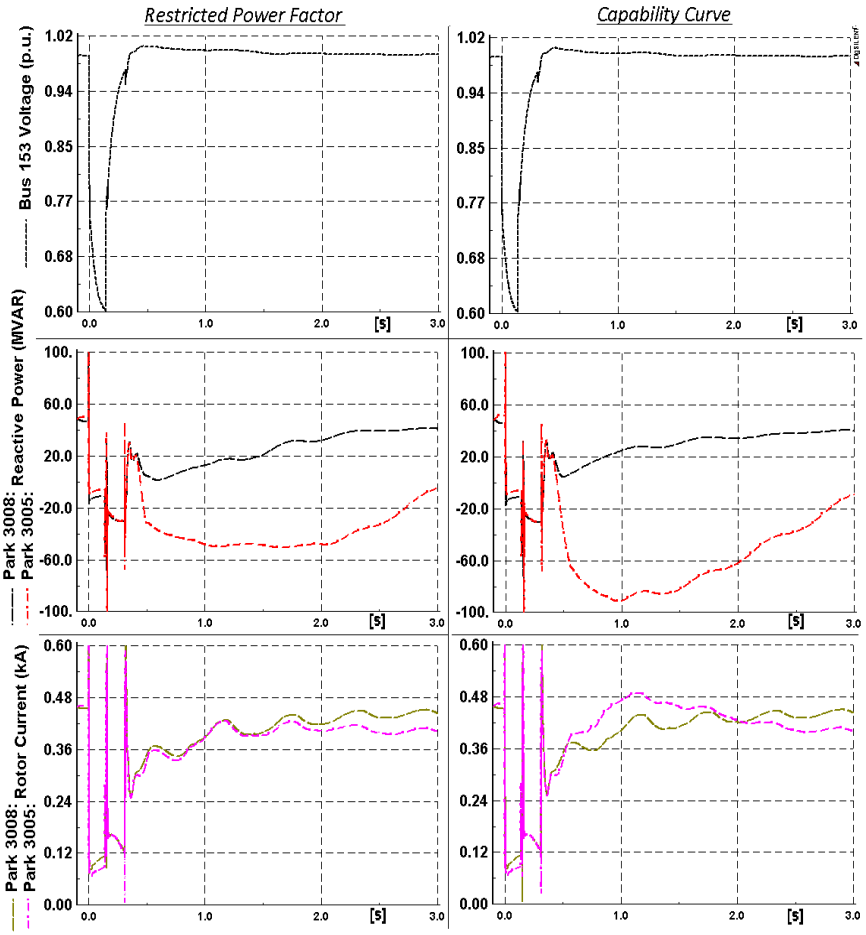

Figure 31. Comparison of bus 153 voltage (p.u.), reactive power (MVAr) (parks: 3008/5 – red/black), and rotor current (kA) (parks: 3008/5 – pink/brown) from 20% penetration at 100% output with RPF (left) and with CC (right) control

Although at 100% plant output the PEC protection triggers and all electrical control of the wind generation (20%) was not active for 0.30 seconds, the system appears relatively unaffected in the short term. In contrast the system experienced it's most dramatic recovery when wind resources were very low and the reactive capability was greatest with the capability curve. Hence, restricting DFIG wind park operation to a fixed power factor range may introduce avoidable reliability risks.

CHAPTER 6. PROJECT CONCLUSIONS

This section will provide a summary to the conclusions drawn from the aforementioned work. Conclusions regarding the static and dynamic performance of enhanced DFIG machines provide the potential to operate a power system more reliably with large penetration levels of wind. This will prove more relevant as the United States looks to become energy independent and more conscious towards the negative impact of increasing emissions from conventional plants.

6.1 Introduction

The operation of DFIG wind parks implementing a capability curve paves the way for regulatory changes. The FERC order 661-A, gives general guidelines for interconnecting wind parks, but for specific parks employing DFIG units the restriction on power factor can be lifted. Fully utilizing the potential of a DFIG wind park may be obtained at no extra cost to the wind farm owner, which not only facilitates increase power transfer margins, but also improves the post fault voltage recovery following a disturbance. As levels of wind penetration continue to increase the responsibility of wind units to adequately substitute conventional machines becomes a critical issue. As demonstrated in this work, amending the fixed power factor regulation to bolster reactive support up to PEC limitations can drastically extend the plants reactive capability at partial loading.

6.1.1 Increased System Transfers

The Voltage Security Assessment laid out in Chapter 4 provided valuable information regarding the determination of an appropriate level of wind penetration for a system. This

systematic approach considered substation voltage levels as stopping criteria and power transfer margins as a metric of comparison. The idea developed for a power system constrained by voltage violations was to strategically place shunt compensation at targeted buses where the violation occurred.

With the aid of the VSA our test system went from having a more reliable base scenario to allowing between 20-25% DFIG wind penetration. This level of wind was then validated with dynamic simulation comprised of a 1.5 MW DFIG wind plant modeled after the GE manufactured machine.

An area of interest that could be pursued further would to include address thermal constraint monitoring into the VSA. How to address the issue of sizing POI transformers due to wind profiles would fall into this category of investigation.

6.1.2 Suggested Order 661-A Revisions

Given advanced SCADA systems and wind forecasting tools it is now possible to receive relatively accurate hour ahead wind generation predictions [46]. This technology is already being incorporated by the California Independent System Operators (CAISO) to schedule generation dispatch around intermittent resources [47]. Under these same principles, operators should also have access to timely information regarding the reactive capability of the plant. This would allow for a more accurate assessment of available reactive power reserves at high penetration levels. Therefore, a policy revision mandating wind park owners to submit plant capability curves to system operators may lend itself to not only more economic dispatch, but also increased stability during voltage emergencies [48].

At the plant level, the Irish grid code maintains a requirement where during a fault the wind park must provide the maximum possible amount of reactive current without violating generator limits [49]. By incorporating this rationale to include the capability curve, a revised U.S. grid code could implicitly define the exact injection to be commanded at the POI for a given operational point. As validated in the simulations, a system can be drastically improved from a farm that regulates its POI voltage. In all four scenarios the controller limits were defined by using the bounds of its capability curve.

The suggested amendments to the current FERC 661-A policy are based on the preceding results. Thus it was demonstrated that the presence of the additional reactive capacity in high penetration scenarios is crucial to enhancing system performance.

APPENDIX A. MAXIMUM POWER TRACKING (MPT) STRATEGY

Doubly fed induction generator wind turbines control their machine's rotational speed to allow operation at maximum power based on the velocity of the wind. This can be accomplished using a power optimization strategy as discussed in [70]. A generic MPT characteristic, based on the GE 1.5 MW wind turbine, was developed for the DFIG wind turbine parks used in this system analysis. Figure 32 presents a graphic with various electrical outputs and generator rotational speeds versus the operational wind speeds with make up the MPT characteristic used in the simulations. The speed range of the machine was designed for a cut-in speed of 3.5 m/s to a cutout wind speed of 25 m/s.

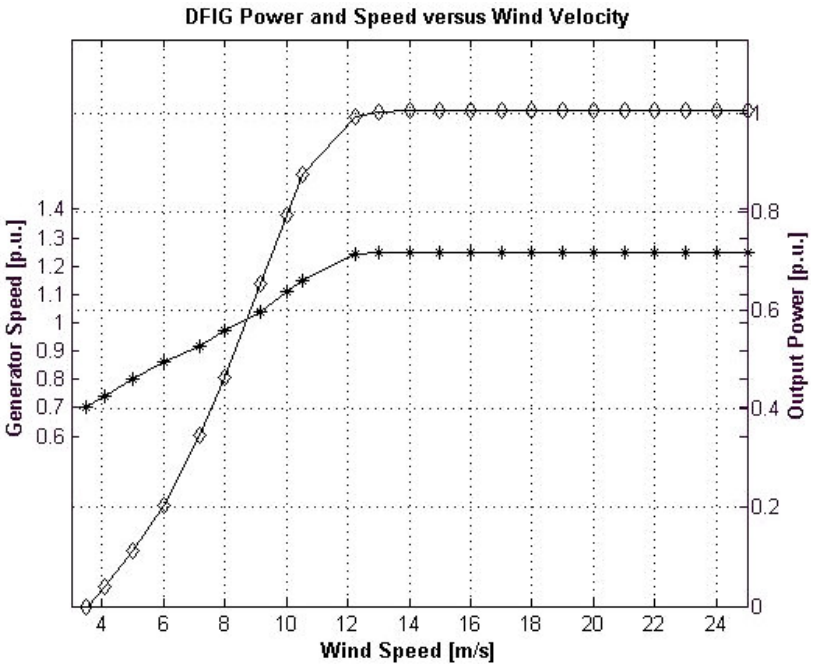

Figure 32. DFIG wind park electrical output (p.u.) and rotor speed (p.u.) versus wind velocity (m/s)

APPENDIX B. MACHINE PARAMETERS

The DFIG model developed for this study was comprised of information gathered from several sources. The model was based around, but not limited to the GE 1.5 MW production DFIG wind turbine. Since proprietary information regarding the exact operation of this machine was not available some inferences were made.

This paragraph explains the origin of the Table 7 simulation parameters and the performance characteristics. The generator electrical parameters were referenced from [31]. The rotor and generator mechanical parameters are defaults from DIgSILENT PowerFactory. The machine parameters (voltage & power ratings, gearbox ratio, etc.) were based on marketing documentation of the GE 1.5 MW wind turbine [69].

Table 7. DFIG Wind Park Machine Simulation Parameters

Rated electrical power	1.5 MW
Rated generator power	1.3 MW
Rated stator voltage	575 V
Rotor to stator turns ratio	3
Machine inertia	30 kgm^2
Rotor inertia	610000 kgm^2
Inductance: mutual, stator, rotor	4.7351, 0.1107, 0.1193 p.u.
Resistance: stator, rotor	0.0059, 0.0066 p.u.
Number of poles	3
Grid frequency	60 Hz
Gearbox ratio	1:72
Nominal rotor speed	16.67 rpm
Rotor radius	42 m
Maximum slip range	+/- 30%

APPENDIX C. PUBLICATIONS

Accepted for publication

R. J. Konopinski, P. Vijayan, V. Ajjarapu, "Extended Reactive Capability of DFIG Wind Parks for Enhanced System Performance", *IEEE Transaction on Power Systems*, 2009

BIBLIOGRAPHY

1. R. Zavadil, N. Miller, A. Ellis, and E. Muljadi, "Making connections," *IEEE Power & Energy Magazine*, pp. 26–37, November/December 2005.
2. R. Doherty, "Establishing the role that wind generation may have in future generation portfolios," *IEEE Transactions on Power Systems,* vol. 21, no. 3, pp. 1415–1422, August 2006.
3. "Industry News: Materials aging and wind," *Power and Energy Magazine, IEEE*, vol.6, no.3, pp.98-99, May-June 2008.
4. U.S. Department of Energy, Energy Efficiency and Renewable Energy, (2008, May). Annual Report on U.S. Wind Power Installation, Cost and Performance Trends: 2007.
5. Trent Berry, Mark Jaccard, "The renewable portfolio standard: design considerations and an implementation survey", *Energy Policy,* vol. 29, no. 4, pp. 263-277, March 2001.
6. Lori Bird, Mark Bolinger, Troy Gagliano, Ryan Wiser, Matthew Brown, Brian Parsons, "Policies and market factors driving wind power development in the United States", *Energy Policy*, vol. 33, no. 11, pp. 1397-1407, July 2005.
7. American Wind Energy Association (AWEA), "Legislative Affairs", Retrieved on 17th July, 2008, from Available: http://www.awea.org/legislative/
8. A.D. Hansen, L H. Hansen, "Wind Turbine Concept Market Penetration over 10 Years (1995-2004)", *Wind Energy*, vol. 10, no.1, pp.81-97, 2007.
9. B. Parsons et al., "Grid Impacts of Wind Power: A Summary of Recent Studies in the United States", *Wind Energy,* vol. 7, no., pp. 87-108, 2004.

10. Y. Chi; Y. Liu; W. Wang; H. Dai, "Voltage Stability Analysis of Wind Farm Integration into Transmission Network," *Power System Technology, 2006. PowerCon 2006. International Conference on*, vol., no., pp.1-7, Oct. 2006
11. P. Kundur, Power System Stability and Control. New York: McGraw-Hill, 1994, pp. 27-33, pp. 209-211.
12. C. W. Taylor, Power System Voltage Stability. New York: McGraw-Hill, 1994, pp. 6-13.
13. V. Ajjarapu, Computational Techniques for Voltage Stability Assessment and Control, New York: Springer Science, 2006, pp. 1-3.
14. A.M. Abed, "WSCC voltage stability criteria, under-voltage, load shedding strategy, and reactive power reserve monitoring methodology," in Proc. IEEE Power Engineering Society Summer Meeting, vol. 1, Edmonton, AB, Canada, Jul. 1999, pp. 191–197.
15. D. Feng, B.H. Chowdhury, M.L. Crow, L. Acar, "Improving voltage stability by reactive power reserve management," *IEEE Trans. on Power Systems,* vol. 20, no.1, pp. 338-345, February 2005.
16. T.J.E. Miller, Reactive power control in electric systems, Wiley, New York (1982), pp. 129-131.
17. T. Van Cutsem, "Voltage instability: Phenomenon, countermeasures and analysis methods," *Proceedings of the IEEE*, vol. 88, no. 2, pp. 208-227, Feb 2000.
18. K. Bhattacharya, J. Zhong, "Reactive Power as an Ancillary Service," *Power Engineering Review, IEEE*, vol. 21, no.5, pp. 64-64, May 2001

19. L. Xu, P. Cartwright, "Direct active and reactive power control of DFIG for wind energy generation," *IEEE Trans. on Energy Conversion*, vol. 21, no. 3, pp. 750-758, Sept. 2006.

20. F.M. Hughes, O. Anaya-Lara, N. Jenkins, G. Strbac, "A power system stabilizer for DFIG-based wind generation," *IEEE Trans. on Power Systems,* vol. 21, no. 2, pp. 763-772, May 2006.

21. G. Tapia, A. Tapia, J.X. Ostolaza, "Proportional–Integral Regulator-Based Approach to Wind Farm Reactive Power Management for Secondary Voltage Control," *IEEE Trans. on Energy Conversion,* vol. 22, no. 2, pp. 88-498, June 2007.

22. Tapia, G. Tapia, J. X. Ostolaza, "Reactive power control of wind farms for voltage control applications", *Renewable Energy*, vol. 29, no. 3, pp. 377-392, March 2004.

23. Federal Energy Regulatory Commission (FERC), Order No. 661 on Interconnection for Wind Farms, June 2, 2005.

24. Federal Energy Regulatory Commission (FERC), Order No. 661A (Order on Rehearing) on interconnection for wind farms, December 12, 2005.

25. Boldea, *Variable Speed Generators*, CRC Press – Taylor & Francis Group, LLC, 2006, p. 1-12.

26. R. Pena, J.C.Clare, G.M. Asher, "Doubly fed induction generator using back-to-back PWM converters and its application to variable-speed wind-energy generation," *Electric Power Applications, IEE Proceedings*, vol. 143, no. 3, pp. 231-241, May 1996.

27. Y. Lei, A. Mullane, G. Lightbody, R. Yacamini, "Modeling of the Wind Turbine With a Doubly Fed Induction Generator for Grid Integration Studies", *IEEE Trans. on Energy Conversion*, vol. 21, no. 1, pp. 257-64, March 2006.

28. J.G. Slootweg, W.L. Kling, "Aggregated modelling of wind parks in power system dynamics simulations," *Power Tech Conference Proceedings, 2003 IEEE Bologna*, vol. 3, no., pp. 23-26, June 2003.

29. M. Poller, S. Achilles, "Aggregated wind park model for analyzing power system dynamics", DIgSILENT Publications, Retrieved on 17th July 2008, from http://www.digsilent.de/Consulting/Publications/

30. DIgSILENT GmH, Manuals, DIgSILENT PowerFactory, Version 13.1., 2004.

31. T. Lund, P. Sorensen, J. Eek, "Reactive Power Capability of a Wind Turbine with Doubly Fed Induction Generator", *Wind Engineering*, no. 10, pp. 379-394, 2007.

32. E. Muljadi, S. Pasupulati, A. Ellis, D. Kosterov, "Method of equivalencing for a large wind power plant with multiple turbine representation," *Power and Energy Society General Meeting - Conversion and Delivery of Electrical Energy in the 21st Century, 2008 IEEE*, vol., no., pp.1-9, 20-24 July 2008

33. M. Kayikci, J.V. Milanovic, "Reactive Power Control Strategies for DFIG-Based Plants," *Energy Conversion, IEEE Transaction on*, vol. 22, no. 2, pp.389-396, June 2007.

34. M.B. Jacobs, "Transmission Recommendations for High Wind Penetration," *Power Engineering Society General Meeting, 2007. IEEE*, vol., no., pp.1-6, 24-28 June 2007

35. National Renewable Energy Laboratory, Golden, CO. [Online]. Available: http://www.nrel.gov/features/04-06_bush.html?print

36. Electric Systems Consultancy, ABB Inc., Wind Farm Integration in British Columbia – Stages 3: Operation Impact, March 28, 2005.

37. "Program Operation Manual", PSSE 30.3.2 Siemens Power Technologies Inc., 2005.

38. "Program Application Guide", PSSE 30.3.2 Siemens Power Technologies Inc., 2005.

39. Peter Van Meirhaeghe, "Double fed induction machine: a EUROSTAG model", *Scientific Publications-Eurostag*, November 2003[Online], Available: http://www.eurostag.be/frameset.htm

40. H.W. Dommel, W.F. Tinney, "Optimal Power Flow", *IEEE Transactions on Power Apparatus and Systems*, October 1968.

41. H. Wang, C. E. Murillo-Sánchez, R. D. Zimmerman, R. J. Thomas, "On Computational Issues of Market-Based Optimal Power Flow", *IEEE Transactions on Power Systems*, Vol. 22, No. 3, Aug. 2007, pp. 1185-1193.

42. "MATPOWER User's Manual", *MATPOWER 3.2 solver* [Online] Available: http://www.pserc.cornell.edu/matpower/

43. R.Piwko, R. DeMello, R. Gramlich, W. Lasher, D. Osborn, C. Dombek, K. Porter, "What Comes First?", *Power and Energy Magazine, IEEE*, vol. 5, no. 6, pp.68-77, Nov.-Dec. 2007.

44. P. Pinson, C. Chevallier, G.N. Kariniotakis, "Trading Wind Generation From Short-Term Probabilistic Forecasts of Wind Power," *Power Systems, IEEE Transactions on*, vol.22, no.3, pp.1148-1156, Aug. 2007

45. A.Fabbri, T.GomezSanRoman, J. RivierAbbad, V.H. MendezQuezada, "Assessment of the Cost Associated With Wind Generation Prediction Errors in a Liberalized

Electricity Market," *Power Systems, IEEE Transactions on*, vol.20, no.3, pp. 1440-1446, Aug. 2005

46. AWS Truewind, http://www.awstruewind.com/
47. Y. Makarov, J. Blatchford, H. Alarian et al., "Incorporation of Wind Power Resources into the California Energy Market", California Independent System Operator Corporation, USA, [Online], Available: http://www.caiso.com/docs/2005/04/05/2005040508370111356.pdf
48. F. Dong, B.H. Chowdhury. M.L. Crow, L. Acar, "Improving Voltage Stability by Reactive Power Reserve Management," *IEEE Transactions on Power Systems*, vol.20, no.1, pp. 338-345, Feb. 2005
49. E. Fagan, S. Grimes, J. McArdle, P. Smith, M. Stronge, "Grid Code Provisions for Wind Generators in Ireland", *Power Engineering Society General Meeting, 2005. IEEE*, pp. 1241-1247, 12-16 June 2005
50. N.E. Nilsson and J. Mercurio, "Synchronous Generator Capability Curve Testing and Evaluation", *IEEE Transactions on Power Delivery*, vol. 9, no.1, January 1994.
51. J.G. Slootweg, S.W. H. de Haan, H. Polinder, W.L. Kling, "Voltage Control Methods with Grid Connected Wind Turbines: a tutorial review", *Wind Engineering*, vol. 25, no. 6, pp. 353-999, 2001
52. T. Ackermann, J.R. Abbad, I. M. Dudurych, I. Erlich, H. Holttinen, J. R. Kristoffersen, P. E. Sorensen, "European Balancing Act", *Power and Energy Magazine, IEEE*, vol. 5, no. 6, pp.91-103, Nov.-Dec. 2007.
53. Western Electricity Coordinating Council, "WECC Reliability Criteria", [Online] *Available*:

http://www.wecc.biz/modules.php?op=modload&name=Downloads&file=index&req=viewdownload&cid=22, April, 2005

54. H. Li, Z. Chen, J.K. Pedersen, "Optimal Power Control Strategy of Maximizing Wind Energy Tracking and Conversion for VSCF Doubly Fed Induction Generator System", *IEEE International Power Electronics and Motion Control Conference*, 2006.
55. DIgSILENT PowerFactory, "Technical Document Dynamic Modeling of Doubly-Fed Induction Machine Wind-Generators", [Online], *Available*: www.digsilent.de/images/Company/news/DFIGRev1.pdf
56. V. Akhmatov, "Variable-Speed Wind Turbines with Doubly-Fed Induction Generators Part III: Model with the Back-to-back Converters", *Wind Engineering*, vol. 27, no.26, pp. 79-91, 2003
57. S. Heier, *Grid Integration of Wind Conversion Systems*, John Wiley & Sons, Inc., 1998, p. 21-34
58. A. Hansen, C. Jauch, P. Sørensen, F. Iov, F. Blaabjerg, "Initialisation of Grid-Connected Wind Turbine Models in Power-System Simulations", Wind Engineering, Vol. 27, No. 1, pp. 21-38, 2003
59. A.D. Hansen, C. Jauch, P. Sorensen, F. Iov, F. Blaabjerg, "Dynamic Wind Turbine Models in System Simulation Tool DIgSILENT", Riso National Laboratory, Riso-R-1400(EN), [Online], Available: www.**digsilent**.de/Software/Application_Examples/ris-r-1400.pdf

60. V. Akhmatov, "Variable-Speed Wind Turbines with Doubly-Fed Induction Generators Part I: Model in Dynamic Simulation Tools", *Wind Engineering*, vol. 26, no.2, pp. 85-108, 2002

61. J.G. Slootweg, H. Polinder, W.L. Kling, "Dynamic Modelling of a Wind Turbine with Doubly Fed Induction Generator", Power Engineering Society Summer Meeting, July 15-19, 2001, IEEE Vol. 1, p. 644 – 649

62. Vladislav Akhmatov, "Analysis of Dynamic Behavior of Electric Power Systems with Large Amount of Wind Power: Phd Thesis", Electric Power Engineering Orsted DTU, April 2003. [Onlin] *Available:* www.elektro.dtu.dk/English/research/eltek/res_projects/-05/va.aspx

63. V. Akhmatov, "Variable-Speed Wind Turbines with Doubly-Fed Induction Generators Part IV: Uninterrupted Operation Features at Grid Faults with Converter Control Coordination", *Wind Engineering*, vol. 27, no.6, pp. 519-529, 2003.

64. I. Erlich, H. Wrede, C. Feltes, "Dynamic Behavior of DFIG-Based Wind Turbines During Grid Faults", *Power Conversion Conference,* pp. 1195-1200*, April 2-5, 2007*.

65. Western Electricity Coordinating Council, "Guide to WECC/NERC Planning Standards I.D: *Voltage Support and Reactive Power*", [Online] *Available*: http://www.wecc.biz/modules.php?op=modload&name=Downloads&file=index&req=viewdownload&cid=22, April, 2005

66. A.D. Hansen, G. Michalke, "Fault Ride-Through Capability of DFIG Wind Turbines", *Renewable Energy*, vol. 32, pp. 1594-1610, 2007.

67. R. Kemsley, G. Pannel, C. Barbier, "Cost Effective Improvements in DFIG Performance Under Fault Conditions for Offshore Applications", Econnect Ventures Ltd. [Online] *Available*: www.berr.gov.uk/files/file40640.pdf

68. Voltage Security Assessment Tool, DSA Tools: Dynamic Security Assessment Tool. [Online] *Available:* http://www.dsatools.com/html/prod_vsat.php

69. 1.5 MW Series Wind Turbine, GE Energy [Online] *Available:* http://www.gepower.com/prod_serv/products/wind_turbines/en/15mw/index.htm

70. H. Li, Z. Chen, J.K. Pedersen, "Optimal Power Control Strategy of Maximizing Wind Energy Tracking and Conversion for VSCF Doubly Fed Induction Generator System", IEEE Power Electronics and Motion Control Conference 2006.

ACKNOWLEDGEMENTS

My fellow ISU graduate power students have contributed much to my educational career at ISU. I appreciated not only all the support I received while working with them, but also their friendships. I would like to acknowledge my committee members, Dr. Gemmill and Dr. Liu, for contributions to this work and also for their wonderful classroom teachings. I am additionally grateful to all ISU faculties, especially in power systems, for bringing about the highest academic standards and challenges.

Most of all I want to recognize Dr. Ajjarapu for graciously welcoming me as one of his researchers. The opportunity he offered me to study at ISU will forever have an impact on my future. For this kind gesture and belief in me, his generosity will not be forgotten.